DISCLAIMER

This report was prepared as an account of work sponsored by an agency of the United States Government. Neither the United States Government nor any agency thereof, nor any of their employees, makes any warranty, express or implied, or assumes any legal liability or responsibility for the accuracy, completeness, or usefulness of any information, apparatus, product, or process disclosed, or represents that its use would not infringe privately owned rights. Reference herein to any specific commercial product, process, or service by trade name, trademark, manufacturer, or otherwise does not necessarily constitute or imply its endorsement, recommendation, or favoring by the United States Government or any agency thereof. The views and opinions of authors expressed herein do not necessarily state or reflect those of the United States Government or any agency thereof. Reference herein to any social initiative (including but not limited to Diversity, Equity, and Inclusion (DEI); Community Benefits Plans (CBP); Justice 40; etc.) is made by the Author independent of any current requirement by the United States Government and does not constitute or imply endorsement, recommendation, or support by the United States Government or any agency thereof.

ORNL/TM-2025/4159

An Overview of the Molten Salt Thermal Properties Database–Thermophysical, Version 4.0 (MSTDB-TP v4.0)

Ryan Chesser
Nicholas Termini
Shane Henderson
Difan Zhang
Vanda Glezakou
Anthony Birri

Approved for public release.
Distribution is unlimited.

September 2025

OAK RIDGE National Laboratory

ORNL IS MANAGED BY UT-BATTELLE LLC FOR THE US DEPARTMENT OF ENERGY

ORNL/TM-2025/4159

Nuclear Energy and Fuel Cycle Division

AN OVERVIEW OF THE MOLTEN SALT THERMAL PROPERTIES DATABASE–THERMOPHYSICAL, VERSION 4.0 (MSTDB-TP V4.0)

Ryan Chesser
Nicholas Termini
Shane Henderson
Difan Zhang
Vanda Glezakou
Anthony Birri

September 2025

Prepared by
OAK RIDGE NATIONAL LABORATORY
Oak Ridge, TN 37831
managed by
UT-BATTELLE LLC
for the
US DEPARTMENT OF ENERGY
under contract DE-AC05-00OR22725

CONTENTS

LIST OF FIGURES

LIST OF TABLES

LIST OF ABBREVIATIONS

API	application programming interface
CMC	critical micelle concentration
CSV	comma separated value
DOE-NE	U.S. Department of Energy, Office of Nuclear Energy
DOI	digital object identifier
GUI	graphical user interface
HDF5	Hierarchical Data Format 5
HPC	high-performance computing
JSON	JavaScript Object Notation
LLM	large language model
MD	molecular dynamics
MOOSE	Multiphysics Object-Oriented Simulation Environment
MOSCATO	Molten Salt Chemistry and Transport
MSR	molten salt reactor
MSTDB	Molten Salt Thermal Properties Database
MSTDB-TC	Molten Salt Thermal Properties Database – Thermochemical
MSTDB-TP	Molten Salt Thermal Properties Database – Thermophysical
NRTL	non-random two liquid
RK	Redlich–Kister
SAM	System Analysis Module
TC	thermochemical
TP	thermophysical

ABSTRACT

A central repository of thermophysical and thermochemical properties of molten salt compositions of relevance to molten salt reactors (MSRs) is vital in supporting the broad community of MSR developers, who are at various stages of developing and deploying their reactor designs. In general, these MSR designs differ significantly from developer to developer (e.g., with respect to the hardness of the neutron spectra, level of fissile loading, target multicomponent temperatures and power levels, and moderating capabilities). Therefore, the fuel and coolant salts being considered vary greatly: they may be chlorides or fluorides, they utilize different actinides at different ratios, and the cations in the melt are selected based on perceived advantages and disadvantages. Considering the general need for thermal properties, and the vastness of the array of potential candidate salt mixtures, the Molten Salt Thermal Properties Database (MSTDB) was initiated in 2018 with the goal of providing thermophysical and thermochemical characterization of key molten salt compounds and mixtures across their temperature and compositional domains. The MSTDB is thus divided into the thermophysical arm (MSTDB-TP) and the thermochemical arm (MSTDB-TC). The MSTDB is an effort funded by the Department of Energy, Office of Nuclear Energy (DOE-NE) Nuclear Energy Advanced Modeling and Simulation (NEAMS) program, and the MSR Campaign.

This report provides an overview of the MSTDB-TP v4.0 in terms of the data contained within, the state of the tools used to access the data, the availability of predictive models that leverage the raw data in the database, the preliminary status of developmental efforts that are currently underway, and an account of future goals for MSTDB-TP. The primary goal for the update from MSTDB-TP v.3.1 to v4.0 was the incorporation of surface tension data into the database; this property is important for thermal hydraulics modeling and species transport in other tools that have been developed under the NEAMS program. A breakdown of the surface tension data that have been added into MSTDB-TP v4.0 is provided herein, and the manner in which the quality of the data has been assessed is also documented. For MSTDB-TP v4.0, newly published thermophysical property data—primarily from collaborative experimental efforts under the MSR Campaign—have been incorporated into the database, and the resulting expansion is documented here. Because of the size to which MSTDB-TP has grown, the raw data format has now been recast into JavaScript Object Notation (JSON) format for easier connection with the MSTDB-TP application programming interface (API), Saline; the pre-existing comma-separated value (CSV) format has been deprecated but is still maintained, accessible, and up to date. As a final effort in packaging the MSTDB-TP v4.0 update, the graphical user interface (GUI) for MSTDB has been updated to allow full accessibility to the density and viscosity predictive models, which are based on Redlich–Kister expansions of MSTDB-TP raw data. Some other major aspects of this report, in terms of preliminary and future work, include: (1) documentation of the formalism and preliminary testing of a kinetic theory model that may act as a predictive model for thermal conductivity; (2) documentation of the candidate predictive models that may be considered in the future for surface tension, making use of the surface tension data now in MSTDB-TP v4.0; (3) a preliminary account of a data collection process that will enable the filling of additional gaps within MSTDB-TP, namely with data which have been collected computationally (e.g., through *ab initio* molecular dynamics).

1. INTRODUCTION

The Molten Salt Thermal Properties Database (MSTDB) is a U.S. Department of Energy, Office of Nuclear Energy (DOE-NE) funded database that includes thermal properties of a wide array of molten salt compounds and multicomponent systems that are candidate materials for molten salt reactor (MSR) coolants and fuels. The database contains two arms, the thermophysical (TP) arm and the thermochemical (TC) arm. Molten Salt Thermal Properties Database – Thermophysical (MSTDB-TP) contains correlations

for key compounds and mixtures that describe thermophysical properties as a function of temperature, whereas Molten Salt Thermal Properties Database – Thermochemical (MSTDB-TC) contains thermodynamic models based on Gibbs energy relations. Both arms and associated documents are hosted on a publicly accessible, permission-protected server at Oak Ridge National Laboratory (ORNL). This report focuses on the current version of MSTDB-TP, but more information regarding MSTDB-TC can be found on the MSTDB website (mstdb.ornl.gov) and in peer-reviewed publications regarding MSTDB-TC and its applications (Ard et al. 2022; Besmann and Schorne-Pinto 2021; Besmann et al. 2024; J. Yingling et al. 2023; Ard et al. 2023; Jacob A Yingling et al. 2023).

The motivation behind the MSTDB-TP is to support thermal hydraulic and multiphysics simulation of MSRs. The chloride and fluoride compounds and multicomponent systems of interest to MSR developers have been outlined in a roadmap for thermal property measurements published in 2021 (Mcmurray et al. 2021). The roadmap has allowed for the formation of a matrix of pseudobinary systems, comprising key molten salt compounds for coolants and fuel that may serve as systems or subsystems of interest for reactors currently under development. Because several designs are currently under development with different fuel and coolant compositions (Krepel and Kramer 2024; Barthle et al. 2024; Roper et al. 2022; Sorensen 2016; Smith et al. 2024; Dolan 2017; Crawford and Lee 2024), it is important to, as exhaustively as possible, fill the existing gaps within this matrix based on experimental and simulated data. Furthermore, the data selected and put into the primary database file—which represents the suggested references for specific molten salt systems by the MSTDB-TP developers—should be the most accurate data to the developers' knowledge. Thus, the MSR design process will not be ill-informed from a thermophysical property standpoint. Therefore, MSTDB-TP developers, in collaboration with external partners (Rose 2022, 2023), have carefully selected single datasets out of duplicate datasets and have chosen to exclude certain datasets for which there exist unique measurements, due to particularly poor experimental controls and highly questionable data.

The MSTDB-TP effort, funded by the DOE-NE Nuclear Energy Advanced Modeling and Simulation (NEAMS) program, has good synergy with the DOE-NE MSR Program. Under the MSR program, several national laboratories are performing thermophysical property measurements that can be incorporated into the MSTDB-TP (Anthony Birri et al. 2023; Karlsson et al. 2023; Rose et al. 2023; Parker et al. 2022; Lonergan et al. 2023; Makovsky et al. 2024; Gardner, Chamberlain, and Rose 2024; Nguyen et al. 2025; Strzelecki et al. 2025). Thus, the database's existing data can be better validated (some of the data are over five decades old), and some of the gaps can be filled, thereby improving the overall understanding of how thermophysical properties change as a function of the compositional space of the chloride and fluoride matrices. Furthermore, molecular dynamics (MD) studies funded under both the MSR and NEAMS programs (Jiang et al. 2024; Andersson and Beeler 2022; Duemmler, Andersson, and Beeler 2024) can provide thermophysical property predictions as well as key insights into why properties may exhibit certain non-ideal trends due to changes in coordination chemistry and ion mobility. While the raw data contained within MSTDB-TP are experimental with a few specific exceptions, it is recognized that the incorporation of the MD-generated thermophysical property data that exist in the literature on thermophysical characterization of molten salts will be crucial.

MSTDB-TP has a variety of user types. As of August 18, 2025, there were a total of 417 users, and the distribution of users and the growth rate of the user base since the MSTDB inception are shown in Fig. 1. Among these users, it is anticipated that some fraction (namely among the national laboratory users) is using MSTDB-TP in high-fidelity simulations of multiphysics, thermal hydraulics, neutronics, or species tracking, based on coupling with a variety of codes that have been developed under NEAMS (Spencer and Besmann 2022). These users benefit from a robust, high-speed interface with the MSTDB-TP to rapidly extract thermophysical property values of need. The user base also includes experimentalists and MD modelers, who generally need limited information from the database and generally seek validation data

to compare against their experiments/models. Finally, private entities may need the MSTDB-TP data for a variety of use cases, including those mentioned already and for design licensing purposes. Given the variety of user types and use cases, MSTDB-TP has both an application programming interface (API) called Saline and a graphical user interface (GUI), which have both been reported previously (Henderson et al. 2021; Termini et al. 2023; T. Birri et al. 2024); updates to these tools are provided herein.

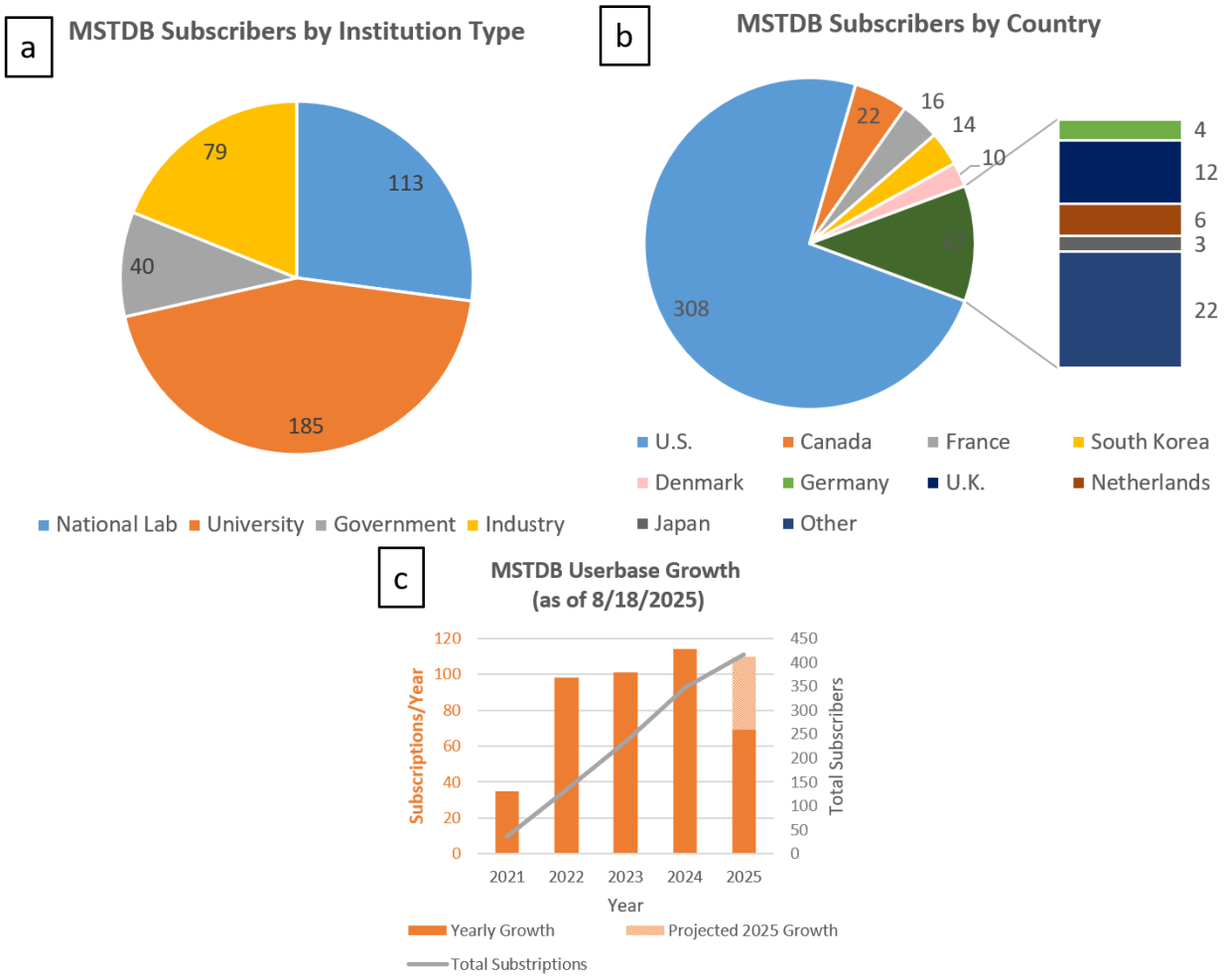

Figure 1. Breakdown of MSTDB subscribers by (a) institution type, and (b) country. Also shown is the (c) total growth and growth rate of MSTDB since its inception.

2. DATABASE COMPOSITION FOR VERSION 4.0

Currently, the TP data held in MSTDB-TP consist of compiled data from 181 published studies conducted by various laboratories, industries, and university projects. The data held in the ORNL GitLab server consist of one JavaScript Object Notation (JSON) file and four comma separated value (CSV) files. The JSON file represents the new manner in which MSTDB-TP data are primarily shared and tracked for version control purposes. Within the JSON file is all the property data for each salt system and their respective compositions, reference data (full references and digital object identifiers (DOIs)), and Redlich–Kister (RK) parameters that are used to generate predictive models for density and viscosity. The CSV files contain the same data that are contained within the JSON file; however, the data are organized such that the raw data, the reference details, the RK parameters for density, and the RK parameters for viscosity are all in separate files. The raw property data for molten salts include the following:

- Melting temperature
- Boiling temperature
- Density
- Viscosity
- Thermal conductivity
- Heat capacity
- Surface tension

For each property, the associated reference, experimentally measured range, empirical constants, and an estimation of the measurement errors are provided. Although all properties are present in the database, each entry (i.e., one specific salt mixture) may not contain all the properties. Property availability for salt mixtures with up to four components is shown in Figs. 2 and 3. Each table or figure shows the salt property data available in the database, as well as the number of measurements over each salt's compositional space that have been recorded for each property.

MSTDB-TP and MSTDB-TC are consistent regarding multicomponent system melting points and pure compound heat capacities. All multicomponent salt systems that have been thermodynamically evaluated by MSTDB-TC v4.0 have had their melting points calculated for MSTDB-TP by the Thermochimica software using the Gibbs energy models in the MSTDB-TC database (except for specific cases where the melting point for a specific salt mixture has been evaluated alongside its thermophysical properties in a given experimental study). Those systems that have not been evaluated by MSTDB-TC v4.0 use existing experimental melting point literature data, if available, for reporting in MSTDB-TP. Heat capacity values for pure compounds have been extracted from the thermodynamic value tabulations within MSTDB-TC, and source references, when available, have been associated. Notably, multicomponent system heat capacities in MSTDB-TP do not mimic MSTDB-TC model outputs; rather, they are extracted directly from experimental values in the literature.

It should be noted that the major change to version 4.0 is the addition of temperature-dependent surface tension data into the database. Surface tension is a key parameter in determining multiphase flow conditions in molten salts because bubble formation, size distribution, and formation of droplets are all dictated by the surface tension of the molten salt (Triplett et al. 1999). In addition, surface tension gives insights into how volatile a salt mixture may be, as the surface tension is inversely related to the vapor pressure (Qiao et al. 2001). Surface tension is relevant to thermal hydraulics applications that have been developed

under NEAMS, and these tools will benefit from storage of such data in MSTDB-TP for streamlined use via the MSTDB-TP API, Saline (Henderson et al. 2021). For example, the drift-flux model that has been built into the Multiphysics Object-Oriented Simulation Environment (MOOSE)–based thermal hydraulics systems application System Analysis Module (SAM) requires surface tension data to quantify the extent to which the velocity of the gas phase differs from the velocity of the bulk fluid (Salko Jr et al. 2021). Another example is the need for surface tension as input for the level-set method within the Molten Salt Chemistry and Transport (MOSCATO) code to track the interface of two-phase flow (Yuan et al. 2024).

Another minor update to the 4.0 version of the database involves the inclusion of several new datasets for thermophysical properties based on experimental measurements taken over the past 1–2 years. These new measurements, which have been captured, have been conducted at both universities and research institutions domestically and internationally. The most prominent, ongoing source of such data is that which has been generated under the DOE-NE MSR Campaign, which is funding the experimental measurement of thermophysical and thermochemical properties of molten salt mixtures relevant to MSRs. It is crucial that MSTDB-TP v4.0 continue to take in this new data so as to fill critical gaps in the database that have been previously uncharacterized. With the combination of new experimental data and surface tension data, the total number of unique salt compositions for which thermophysical property data have been evaluated in MSTDB-TP v4.0 stands at 976 entries.

2.1 SURFACE TENSION DATA DETAILS

Surface tension correlations for pure and multicomponent chlorides and fluorides were incorporated into MSTDB-TP v4.0 based on published literature. The correlations for surface tension each follow a linear temperature trend where A and B are constants fitted to experimental data, T is the temperature in $Kelvin$, and γ is the surface tension in dyn/cm, given by:

$$\gamma = A - BT \quad . \tag{1}$$

MSTDB-TP reports these fitted constants along with applicable temperature ranges and reported/assessed measurement uncertainty for each system and each composition. Selected correlations were chosen based on a six-factor quality assessment developed by Rose (2022). The six factors of quality assessment include method, calibrations, salt composition analysis, environmental controls, measurement precision, and verifiable property values. Each factor is given a high, moderate, or incomplete ranking based on the level of detail that the reference provides regarding that factor (see Table 2). For example, a reference providing quantified uncertainty based on at least three replicate measurements may be given a high quality ranking in measurement precision; providing a propagated uncertainty or uncertainty budget based on individual measurements may be given a moderate quality ranking; and no measured or estimated uncertainty reporting would be given an incomplete ranking. For each reported salt system, the selected correlation was chosen based on the highest combined score across each quality assessment factor.

A list of each salt system with correlations in MSTDB-TP v4.0 is given in Table 1. For multicomponent systems, the total number of unique compositions is also provided. For chloride salts, there are 16 pure component systems, 9 binary systems totaling 53 unique compositions, and 1 ternary system totaling 17 unique compositions. For fluoride salts, there are 13 pure component systems, 10 binary systems totaling 55 unique compositions, 7 ternary systems totaling 74 unique compositions, and 2 quaternary systems totaling 66 unique compositions. For each unique composition, one reference correlation was selected for incorporation into the database based on the criteria described above. This resulted in a total of 86 correlations for unique chloride compositions based on 121 reported measurements, and 208 correlations for unique fluoride compositions based on 88 reported measurements.

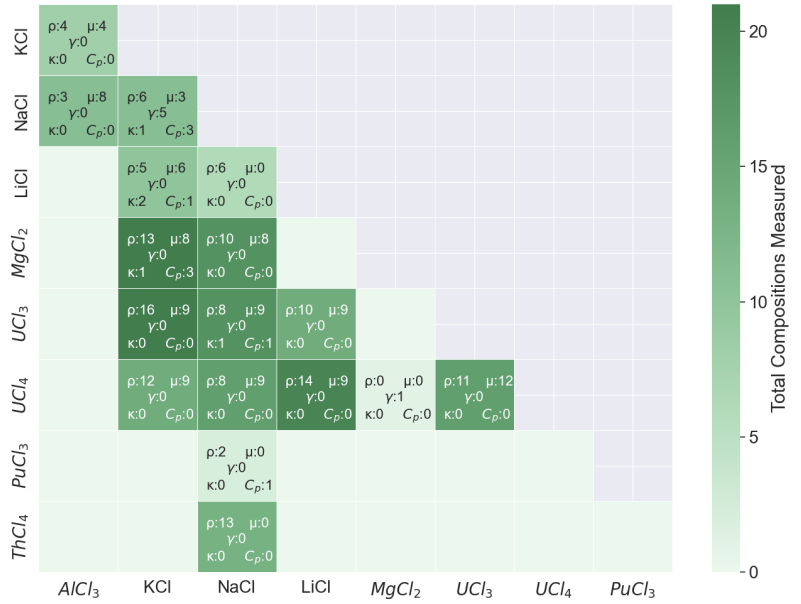

Chloride pseudobinary salts

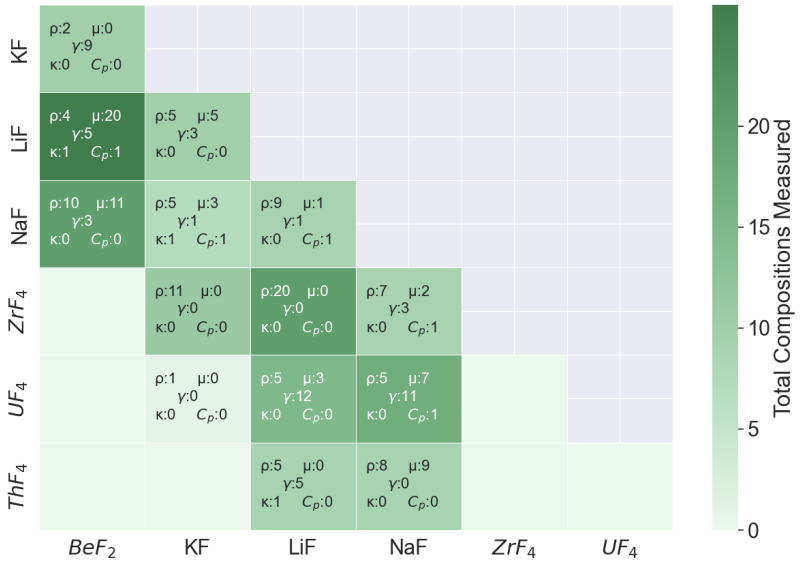

Fluoride pseudobinary salts

Figure 2. Heat map of measured properties for chloride and fluoride pseudobinary salts in MSTDB-TP v4.0.

Salt	ρ	μ	κ	c_p	γ
AlCl3	1	1	0	1	0
BeCl2	1	0	0	0	0
BeF2	1	1	1	1	0
CaCl2	1	1	1	1	1
CaF2	1	1	1	1	1
GdCl3	1	1	0	0	1
GdF3	0	0	0	0	0
KCl	1	1	1	1	1
KF	1	1	1	1	1
LaCl3	1	1	0	0	1
LaF3	1	0	0	1	0
LiCl	1	1	1	1	1
LiF	1	1	1	1	1
MgCl2	1	1	1	1	1
MgF2	1	1	1	0	1
NaCl	1	1	1	1	1
NaF	1	1	1	1	1
NdCl3	1	1	0	0	1
NdF3	0	0	0	1	0
NpCl3	0	0	0	0	0
NpF3	0	0	0	0	0
PuCl3	0	0	0	1	0
PuF3	0	0	0	1	0
SrCl2	1	1	1	0	1
SrF2	1	1	1	0	1
ThCl4	1	0	0	0	0
ThF4	1	0	0	0	1
UCl3	1	1	0	1	1
UCl4	1	1	0	0	1
UF3	0	0	0	1	0
UF4	1	1	0	1	1
ZrCl4	1	1	0	0	0
ZrF4	1	0	0	0	1
RbCl	0	0	0	0	1
CsCl	0	0	0	0	1
BaCl2	0	0	0	0	1
PrCl3	0	0	0	0	1
RbF	0	0	0	0	1
CsF	0	0	0	0	1
BaF2	0	0	0	0	1
UF6	0	0	0	0	1

Salt	ρ	μ	κ	c_p	γ
AlCl3-LiCl-NaCl	10	10	0	0	0
BeF2-KF-NaF	1	1	0	1	0
BeF2-LiF-NaF	5	4	0	5	0
BeF2-LiF-ThF4	3	2	0	0	44
BeF2-LiF-UF4	36	38	2	0	1
BeF2-LiF-ZrF4	1	0	0	0	0
BeF2-NaF-UF4	78	70	0	0	1
KCl-LiCl-NaCl	4	0	0	0	0
KCl-LiCl-UCl3	18	0	0	0	0
KCl-LiCl-UCl4	18	0	0	0	0
KCl-MgCl2-NaCl	1	1	1	1	0
KCl-NaCl-UCl3	18	20	0	1	0
KCl-UCl3-UCl4	32	0	0	0	0
KF-LiF-NaF	1	1	1	1	1
KF-MgF2-NaF	1	0	1	1	0
KF-NaF-UF4	4	2	3	3	0
KF-NaF-ZrF4	1	1	0	1	0
NaCl-PuCl3-UCl3	3	0	0	0	0
MgCl2-NaCl-PuCl3	2	0	0	0	0
LiCl-NaCl-UCl3	18	0	0	0	0
LiCl-NaCl-UCl4	18	0	0	0	0
LiCl-UCl3-UCl4	21	0	0	0	0
LiF-NaF-ZrF4	10	1	1	2	11
LiF-ThF4-UF4	1	0	0	0	0
NaCl-UCl3-UCl4	21	40	0	0	0
NaF-UF4-ZrF4	5	4	0	6	0
RbF-UF4-ZrF4	2	2	0	2	0
CaCl2-LaCl3-NaCl	0	0	0	0	1
CaF2-LiF-NaF	0	0	0	0	1
KF-LiF-ZrF4	0	0	0	0	1

Salt	ρ	μ	κ	c_p	γ
BeF2-LiF-NaF-UF4	1	1	0	1	0
BeF2-LiF-ThF4-UF4	1	1	1	1	32
BeF2-LiF-UF4-ZrF4	1	0	1	0	0
BeF2-NaF-UF4-ZrF4	1	0	0	0	0
KF-LiF-NaF-UF4	2	2	0	2	0
KF-NaF-UF4-ZrF4	0	0	0	2	0
LiF-NaF-UF4-ZrF4	1	1	0	2	0
BeF2-NaF-ThF4-UF4	0	0	0	0	1

Figure 3. Tables of the number of measured properties in MSTDB-TP v4.0 for pure, pseudoternary, and pseudoquaternary salts.

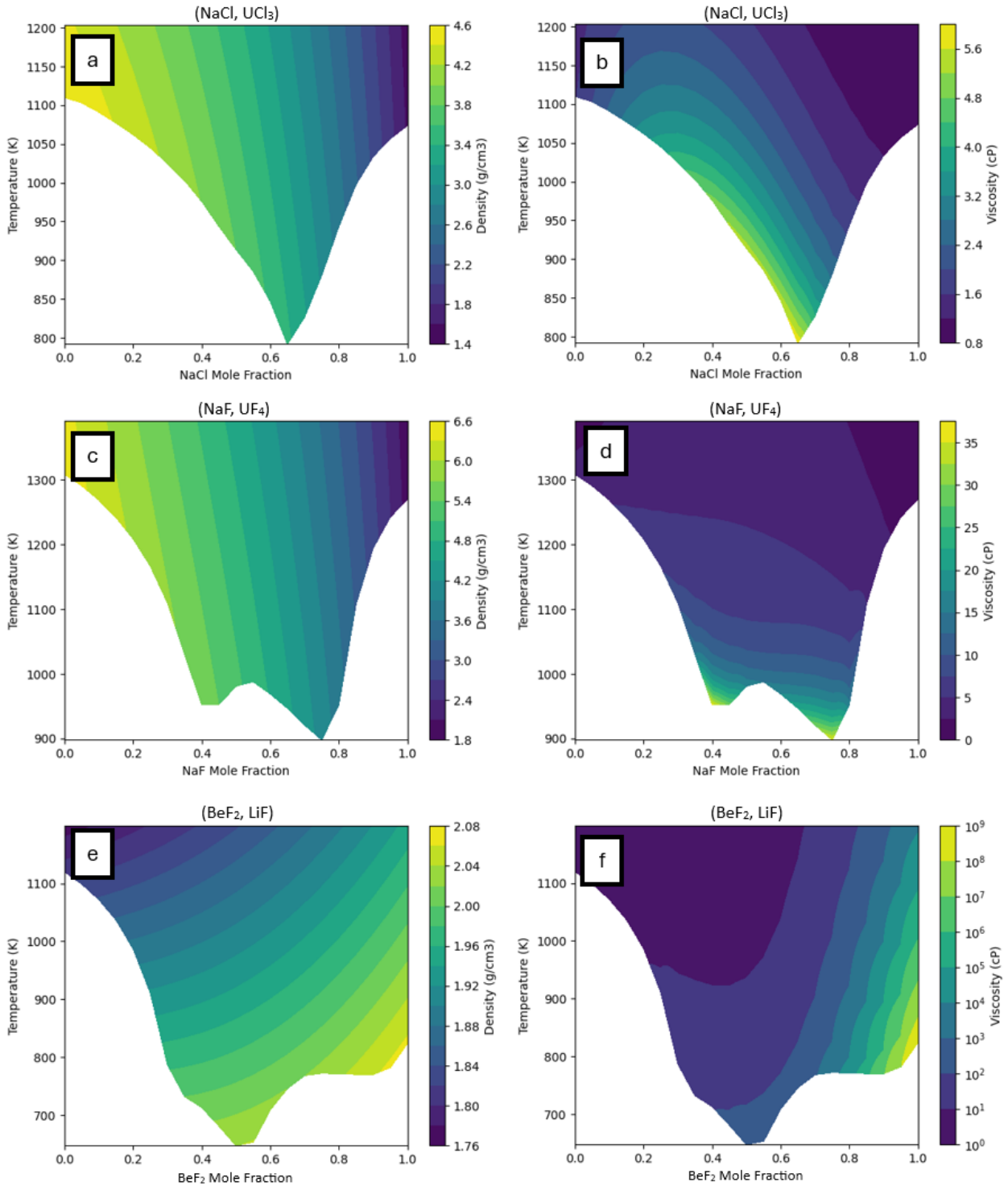

Figure 4. Density and viscosity data as calculated based on the RK parameters summarized in Tables 3 and 4. The subfigures contain (a) density data for NaCl-UCl_3, (b) viscosity data for NaCl-UCl_3, (c) density data for NaF-UF_4, (d) viscosity data for NaF-UF_4, (e) density data for LiF-BeF_2, and (f) viscosity data for LiF-BeF_2.

Table 1. Salt systems with correlations in MSTDB-TP v4.0 for surface tension.

Chloride Salt System	Number of Compositions (Number of Studies)	**Fluoride Salt System**	Number of Compositions (Number of Studies)
LiCl	– (11)	LiF	– (10)
NaCl	– (20)	NaF	– (10)
KCl	– (18)	KF	– (7)
RbCl	– (7)	RbF	– (5)
CsCl	– (8)	CsF	– (4)
$MgCl_2$	– (5)	MgF_2	– (4)
$CaCl_2$	– (6)	CaF_2	– (8)
$SrCl_2$	– (1)	SrF_2	– (3)
$BaCl_2$	– (3)	BaF_2	– (4)
$LaCl_3$	– (5)	ZrF_4	– (2)
$PrCl_3$	– (2)	ThF_4	– (1)
$NdCl_3$	– (1)	UF_4	– (1)
$GdCl_3$	– (1)	UF_6	– (1)
$DyCl_3$	– (1)	LiF-KF	3 (1)
UCl_3	– (1)	LiF-NaF	1 (1)
UCl_4	– (3)	LiF-BeF_2	7 (3)
NaCl-KCl	5 (3)	LiF-UF_4	12 (1)
NaCl-$CaCl_2$	6 (1)	LiF-ThF_4	5 (1)
NaCl-$LaCl_3$	5 (1)	NaF-KF	1 (1)
NaCl-$PrCl_3$	5 (1)	NaF-BeF_2	3 (2)
KCl-$PrCl_3$	5 (1)	NaF-ZrF_4	3 (1)
$MgCl_2$-UCl_4	7 (1)	NaF-UF_4	11 (1)
$CaCl_2$-$LaCl_3$	5 (1)	KF-BeF_2	9 (1)
$CaCl_2$-$PrCl_3$	6 (1)	LiF-NaF-KF	1 (4)
$CaCl_2$-UCl_4	9 (1)	LiF-NaF-CaF_2	1 (1)
NaCl-$CaCl_2$-$LaCl_3$	17 (1)	LiF-NaF-ZrF_4	11 (1)
		LiF-KF-ZrF_4	10 (1)
		LiF-BeF_2-UF_4	1 (1)
		LiF-BeF_2-ThF_4	49 (2)
		NaF-BeF_2-UF_4	1 (1)
		LiF-BeF_2-UF_4-ThF_4	33 (2)
		NaF-BeF_2-UF_4-ThF_4	33 (2)

For systems with more than one published data set, the selected reference correlation is chosen by comparing the quality ranking score of each data set. For each of the six quality aspects in Table 2, high quality is given 3 points, moderate quality is given 2 points, and insufficient quality is given 1 point. Summing the score of each quality aspect yields a final quality score in the range of 6–18. If multiple data sets tie for the highest quality score, then the decision is made by secondary factors such as the number and density of data points, lowest reported uncertainty, and largest measured temperature range. Figure 5 below provides a typical example of duplicate data sets for a given species—in this case, lithium chloride.

2.2 RK PARAMETERS FOR DENSITY AND VISCOSITY

RK models have been developed for both density and viscosity for interpolation within the temporal and compositional space for pseudobinary systems, as well as extrapolation to higher-order systems based on pseudobinary subsystems. The mathematical formalisms are derived in previous publications (Agca and McMurray 2022; A. Birri et al. 2022; T. Birri et al. 2024). Ultimately, in the RK formalism, the density (ρ) and viscosity (η) are defined by

$$\rho = \rho_{id} + \rho_{ex} \tag{2}$$

Table 2. Quality ranking criteria (based on Rose (2023)) for published literature in MSTDB-TP used in the selection of reference correlations.

Quality Aspect	High Quality (H)	Moderate Quality (M)	Insufficient Quality (I)
Method	Standardized method for application to molten salts with international consensus	Well-established method employed at several laboratories	Documented procedure unique to small number of laboratories
Calibrations	Verification of proper instrument performance based on response of reference material and calibration of all instruments used to determine property value with certified standards	Verification of proper instrument performance based on response of reference material or calibration of all instruments used to determine property value with certified standards	Sufficient calibration results not provided
Composition	Replicate analyses of complete salt composition including cations, anions, and impurities, or controlled batching of known mixture under a controlled atmosphere	Replicate analysis for major cation salt constituents (typically > 3 mol %) and impurities prior to measurement	No analyses or only analysis for major cation salt constituents (typically > 3 mol %) prior to measurement
Environment Control	Confirmed control and stability of temperature and atmosphere during measurement	Measured salt or furnace temperature prior to measurement and limited control of atmosphere	Environmental controls not reported
Measurement Precision	Quantified uncertainty based on at least three replicate measurements	Propagated uncertainty or uncertainty budget based on individual measurements	No measured or estimated uncertainty reported
Verifiability	Measured data and determined property value provided and verifiable	Both measured data and determined property value provided	Insufficient information available to verify reported value

and

$$\ln(\eta) = \ln(\eta_{id}) + \ln(\eta_{ex}), \tag{3}$$

where ρ_{id} is the ideal mixture density (assuming ρ is being evaluated for a salt system with an order of 2 or greater), ρ_{ex} is the excess (or non-ideal) mixture density, η_{id} is the ideal mixture viscosity (assuming η is being evaluated for a salt system with an order of 2 or greater), and η_{ex} is the excess (or non-ideal) mixture viscosity. Note that both ρ and η are functions of temperature and composition.

The ideal models chosen for MSTDB-TP v4.0 are

$$\rho_{id} = \Big(\sum_i x_i M_i\Big) \Big/ \sum_i \frac{x_i M_i}{\rho_i} \tag{4}$$

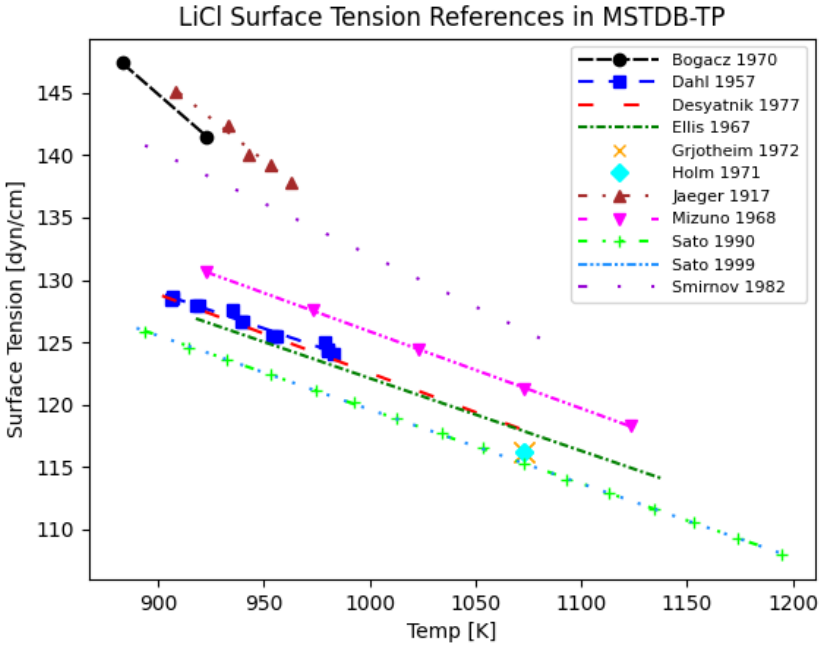

Figure 5. Data for surface tension of LiCl reported by eleven publications available in MSTDB-TP.

and

$$\ln(\eta_{id}) = \sum_i x_i \ln(\eta_i), \tag{5}$$

where x_i, M_i, ρ_i, and η_i are the molar fraction, molar mass, density, and viscosity of the i^{th} mixture constituent, respectively. The excess terms in Eqs. (2) and (3) are dictated by RK expansions. Therefore, for any pseudobinary system (or subsystem) with compositions x_1 and x_2, these excess terms are defined by

$$\rho_{ex} = x_1 x_2 \sum_{j=1}^{n} L_j^{12} (x_1 - x_2)^{j-1} \tag{6}$$

and

$$\ln(\eta_{ex}) = x_1 x_2 \sum_{j=1}^{n} L_j^{12} (x_1 - x_2)^{j-1}. \tag{7}$$

The temperature-dependent constants in the non-ideal components of the model, L_j^{12}, are defined by

$$L_j^{12} = A_j^{12} + B_j^{12} T \tag{8}$$

for density and

$$L_j^{12} = A_j^{12} + B_j^{12} T + C_j^{12} T^2 \tag{9}$$

for viscosity.

The total list of RK parameters in the MSTDB-TP v4.0 for density and viscosity is provided in Tables 3 and 4.

Table 3. RK parameters in MSTDB-TP v4.0 for density estimation.

Salt 1	Salt 2	A_1^{12} (g/cm^3)	B_1^{12} (g/cm^3K)	A_2^{12} (g/cm^3)	B_2^{12} (g/cm^3K)
KCl	NaCl	−0.03013	-1.210×10^{-5}	0	0
KCl	$MgCl_2$	0.3931	-4.92×10^{-4}	0	0
KCl	UCl_3	−2.121	0.001491	1.569	−0.001689
KCl	UCl_4	−2.333	0.002062	0.5056	2.12×10^{-5}
KCl	KF	0.08214	-7.36×10^{-5}	0	0
KCl	ZrF_4	−1.906	6.93×10^{-4}	2.227	-0.001029
KF	LiF	−0.05708	2.90×10^{-5}	0	0
KF	ZrF_4	−1.774	5.79×10^{-4}	0.9944	-2.61×10^{-4}
LiCl	KCl	0.0768	-8.50×10^{-5}	0	0
LiCl	UCl_3	−1.525	0.001506	1.321	−0.001584
LiCl	UCl_4	−1.956	0.001796	1.404	-9.84×10^{-4}
LiF	BeF_2	−0.2616	7.53×10^{-5}	0	0
LiF	ThF_4	1.769	−0.001047	−1.798	8.73×10^{-4}
LiF	UF_4	2.219	−0.00177	−2.7853	0.002645
LiF	ZrF_4	−1.272	-4.87×10^{-4}	0.7348	2.31×10^{-4}
NaCl	$ThCl_4$	−0.2744	3.90×10^{-4}	0	0
NaCl	UCl_3	−0.1333	1.44×10^{-4}	0	0
NaCl	UCl_4	−2.8509	0.002824	3.025	−0.002985
NaCl	NaF	−0.117	1.77×10^{-5}	0	0
NaCl	ZrF_4	−1.0393	3.57×10^{-4}	−0.04282	1.84×10^{-4}
NaF	KF	−0.6499	2.97×10^{-4}	0	0
NaF	LiF	0.005952	-5.25×10^{-5}	0	0
NaF	ThF_4	0.4476	-7.62×10^{-4}	0	0
NaF	UF_4	−0.1274	-8.07×10^{-4}	0	0
NaF	ZrF_4	−1.2952	3.1×10^{-4}	−0.4568	6.65×10^{-4}
NaF	BeF_2	0.009154	-1.06×10^{-4}	0	0
UCl_3	UCl_4	0.1833	2.61×10^{-4}	0	0

Table 4. Redlich–Kister parameters in MSTDB-TP v4.0 for viscosity estimation.

Salt 1	Salt 2	A_1^{12} (g/cm^3)	B_1^{12} (g/cm^3K)	C_1^{12} (g/cm^3K^2)	A_2^{12} (g/cm^3)	B_2^{12} (g/cm^3K)	C_2^{12} (g/cm^3K^2)
KCl	NaCl	1.931	−0.001878	0	−1.0121	-4.04×10^{-5}	0
KCl	$MgCl_2$	−4.258	0.005012	-1.66×10^{-6}	−6.125	0.009048	-3.00×10^{-6}
KCl	UCl_3	16.96	−0.0203	6.26×10^{-6}	−32.46	0.0400	-1.24×10^{-5}
KF	LiF	−0.6398	-2.80×10^{-4}	0	0	0	0
LiCl	KCl	−0.7936	6.61×10^{-4}	0	0	0	0
LiF	UF_4	−101	0.141	-4.71×10^{-5}	78.82	−0.1039	3.33×10^{-5}
NaF	KF	0.7318	-7.19×10^{-4}	0	−0.34734	5.99×10^{-4}	0
NaCl	$MgCl_2$	−0.1719	-7.55×10^{-4}	2.30×10^{-7}	−3.753	0.004986	-1.52×10^{-6}
NaCl	UCl_3	21.44	−0.02594	7.95×10^{-6}	−25.24	0.0301	-9.24×10^{-6}
LiCl	UCl_3	10.57	−0.01094	3.47×10^{-6}	−8.417	0.01062	-3.36×10^{-6}
NaCl	UCl_4	−4.008	0.005072	0	10.47	−0.008681	0
LiCl	UCl_4	−9.083	0.017	-5.65×10^{-6}	12.26	−0.01762	5.85×10^{-6}
KCl	UCl_4	−7.557	0.0132	-4.72×10^{-6}	20.08	−0.0267	9.52×10^{-6}
UCl_3	UCl_4	24.63	−0.02749	8.50×10^{-6}	17.13	−0.0208	6.42×10^{-6}
NaF	LiF	0.1938	-1.55×10^{-4}	0	0	0	0
NaF	UF_4	−130.6	0.1864	-6.44×10^{-5}	124.2	−0.169	5.72×10^{-5}
NaF	BeF_2	−97.66	0.1081	-3.29×10^{-5}	36.368	−0.0309	9.42×10^{-6}
LiF	BeF_2	−97.41	0.1043	-2.90×10^{-5}	104.354	−0.117	3.25×10^{-5}

In order to provide a visualization of how these RK models change as a function of composition and temperature, the estimated densities and viscosities are plotted in Fig. 4 for three very relevant pseudobinary salt systems to the developing MSR industry; NaCl-UCl_3, NaF-UF_4, and LiF-BeF_2. These salt systems are relevant for chloride fast reactor designs, and fluoride reactor designs with either thermal or fast spectra, and different levels of fuel loading. Regarding NaCl-UCl_3, the RK parameters have been determined based on data from Parker (Parker et al. 2022) for density, and Katyshev (Katyshev 2001) for viscosity; for NaF-UF_4, the RK parameters have been determined based on data from Blanke for density (Blanke, Bousquet, et al. 1958) and for viscosity (Blanke, Foster, et al. 1958); for LiF-BeF_2, the RK parameters have been determined based on data from Cantor, Ward, and Moynihan (1969) and Cantor (1973) for density and viscosity. The liquidus projections from MSTDB-TC v4.0 have been utilized to determine valid temperature ranges over which the thermophysical properties in Fig. 4 have been plotted (J. Yingling et al. 2023; Besmann and Schorne-Pinto 2021).

2.3 RAW DATA FORMAT OPTIONS

With the addition of surface tension data and additional estimation options to MSTDB-TP it became clear that the existing CSV would not scale well with the database's intended use(s). Since the format would already be forced to change to incorporate surface tension data, it was decided to encode the data in the JSON format. For a formal description of JSON refer to standards, ECMA-404 and ISO/IEC 21778, and/or the current RFC. At this writing, RFC 8259 is used. This does not mean that the CSV is obsolete; however, new properties may not be added to the CSV as quickly as to the JSON.

In accordance with (Bray 2017), "names within an object SHOULD be unique." For MSTDB-TP this requirement is elevated to SHALL, ensuring that ambiguity cannot occur. Further, objects with unique names are guaranteed to be interoperable, which promotes shared understanding of what MSTDB-TP JSON objects represent.

The improvement in interoperability reduces the burden of "data cleaning" for the maintainers because we can use commonly available tooling to both check and enforce MSTDB-TP format, but a consequence is that only one entry will exist per composition, which precludes the possibility of inadvertently shadowing data during data entry. Overall, the integrity of the database is improved and simultaneously made intuitive for downstream clients.

A further advantage brought by JSON is the flexibility to name and add pieces of data that are not currently implemented or not necessarily implemented by all tools. This was impossible in CSV format, as the addition of a column required every implementation to implement that column. The analogous key in JSON is simply ignored until a client requires it, at which point it is only required for that client.

Finally, JSON promotes translation to a similarly hierarchical format, Hierarchical Data Format 5 (HDF5). Although the HDF5 format is currently not heavily promoted, it provides an option for implementing the data in a manner that promotes high-performance computing (HPC) modeling efforts. The hierarchical nature of both JSON and HDF5 promote integration of data via various models that may not have been encountered yet, especially for the purposes of estimating unmeasured compositions.

3. PREDICTIVE CAPABILITIES IN DATABASE TOOLS

3.1 REDLICH–KISTER DATA STORE OPTION IN SALINE

The addition of viscosity RK data to MSTDB-TP prompted changes to the RK viscosity implementation in Saline. Previous efforts to use Saline's estimation capability with viscosity would utilize ideal mixing. When the new interpolation parameters are available, the model now calculates an "excess mixing term" that improves the expected accuracy of the estimation.

Alongside this change, a slight modification to Saline's default behavior has been made. In previous iterations, if Saline could find the exact composition in experimental data, then it would not attempt to make an estimate. After considering the various use cases, this behavior is generally not desirable.

Consider the case in which a client is making a series of estimations as part of a scoping or sensitivity study. When they stumble upon an exact match, Saline could report a step change compared to surrounding values. Even though the RK implementation is often within the margin of error, the magnitude of error could still skew results. To prevent the user from experiencing any discontinuity, the RK implementation now only uses experimental data as input to its own models. A future feature being planned is incorporating a tuning parameter that allows clients to decide whether and when an experimental value would be used directly.

3.2 GRAPHICAL USER INTERFACE: PREDICTION TAB

In an effort to provide RK estimation capabilities to a wider user base, RK density and viscosity models are implemented into the MSTDB-TP GUI. This is done using the RK-DataStore module through Saline in Python. A snapshot of the estimation tab is shown in Figure 6 calculating the RK estimated density of various NaCl/KCl/LiCl combinations at 1000 K.

If RK parameters are not available for the chosen binary/ternary, an ideal mixing density value will be calculated instead. Compositional plots can be produced at different isotherms for both viscosity and density using RK or ideal mixing extrapolation, demonstrated by the "RK" or "Ideal" next to the binary. Ternary RK extrapolation uses a combination of binary interaction parameters, so the degree to which ideal mixing or RK extrapolation is used in the estimation of ternary parameters depends on the binaries themselves. Contour plots of composition vs. temperature will be produced for binaries if MSTDB-TC data exist to calculate relevant melting temperatures, and any data calculated below the melting point for a given composition will be excluded. If no MSTDB-TC models exist for the selected compound, then single isotherms will be plotted over a compositional range instead of a contour plot for binaries. Both isotherms to be plotted, and compositional ranges, can be changed by the user. Examples of the different plots produced by the GUI are shown in Fig. 7.

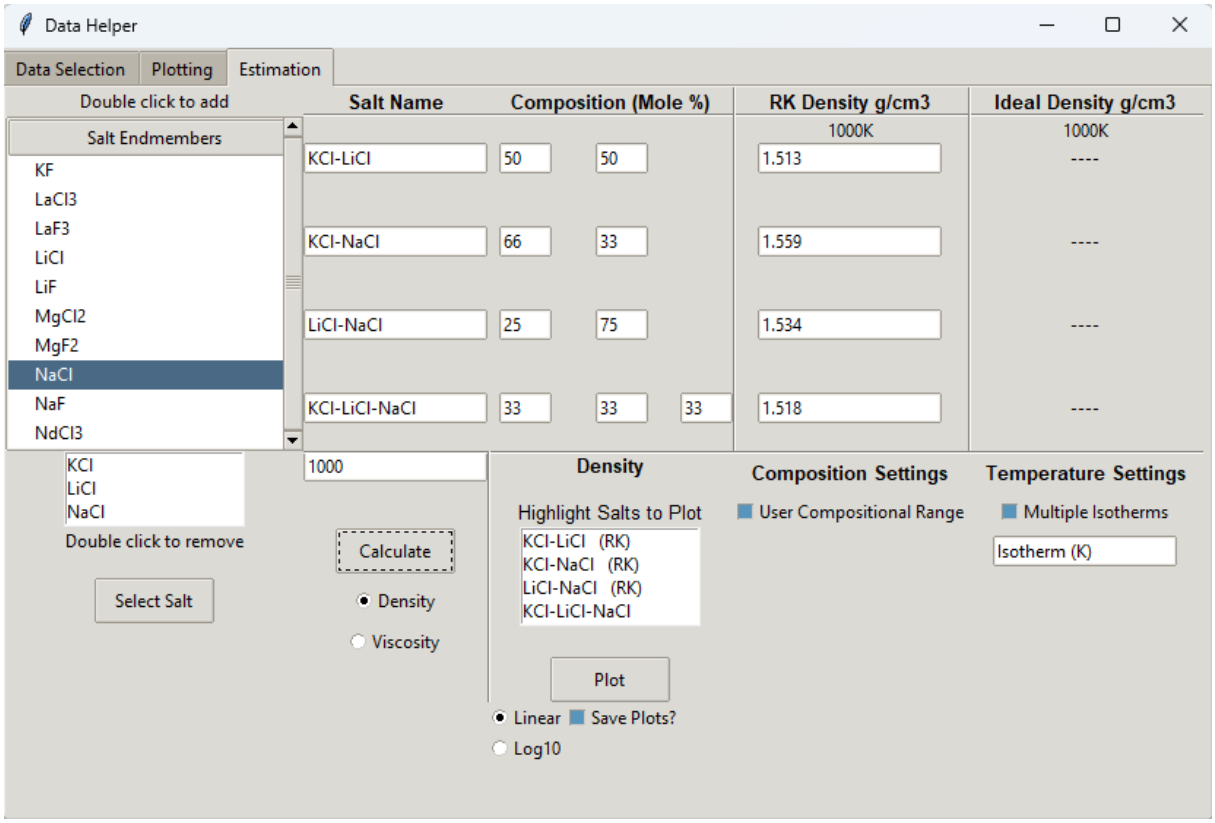

Figure 6. Snapshot of MSTDB-TP GUI showing the calculation of different compositions at a single temperature.

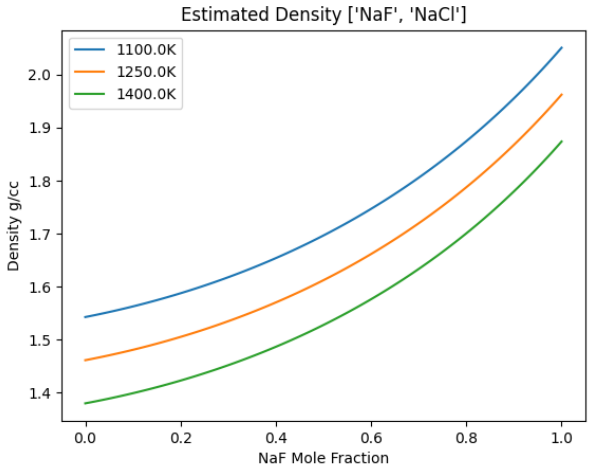

Binary plotting of three isotherms

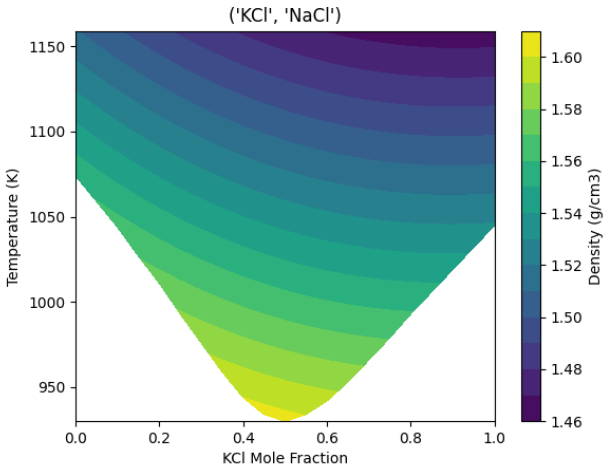

Binary contour plotting above melting point

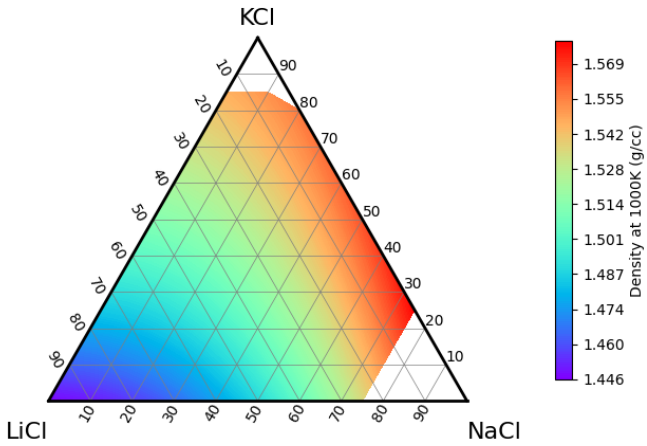

Ternary density contour plotting excluding compositions with a higher melting point

Figure 7. RK estimated density plots of three different styles.

4. THERMAL CONDUCTIVITY PREDICTIVE MODEL

4.1 BACKGROUND ON KINETIC THEORY

While the RK formalism has worked well for generating predictive models for densities and viscosities by utilizing MSTDB-TP data, this formalism is not extensible to thermal conductivity for one primary reason; there is not enough reliable thermal conductivity data available to develop compositionally dependent non-ideal terms within a RK expansion. Yet, predictive modeling capabilities are direly needed to support MSTDB-TP such that critical data gaps can be estimated, in support of design and modeling efforts associated with MSRs. Fortunately, there is one particular formalism by Gheribi which has been developed and well-validated against alkali and alkaline earth halides, based on kinetic theory (Gheribi, Torres, and Chartrand 2014; Gheribi, Salanne, and Chartrand 2016; Gheribi, Phan, and Chartrand 2022; Gheribi et al. 2024).

Fundamentally, the kinetic theory approach to modeling molten salt thermal conductivity is based on phononic energy transfer, such that the formalism mimics that of amorphous solids which do have short-range order. The model relies on knowledge of the bulk heat capacity (which can be measured), the speed of sound (which can also be measured), and the mean free path of a phonon (which can be estimated in several ways, based on different underlying assumptions). The power of this model is that mixture data are not inherently needed; both heat capacity and speed of sound can be estimated based on endmember experimental measurements, while the mean free path of a phonon is an entirely modeled parameter, either for pure compounds or mixtures. This opens up the possibility of using a kinetic theory model as a predictive model in support of MSTDB-TP, even though thermal conductivity data on mixtures is particularly sparse. Of course, the main challenge is that kinetic theory has not really been applied to actinide halides in the literature, and thus it is the goal within this report to demonstrate how the kinetic theory model(s) put forth in the literature may be modified so that the overall model is generalizable to molten salts which may or may not bear actinides.

4.2 FORMALISM FOR THE GENERALIZABLE MODEL

The first step to generating a thermal conductivity model for molten salt mixtures involves defining the thermal conductivity of individual compounds (with index i) which may be mixed together in a multicomponent system. The thermal conductivity of compound i can be expressed as (Gheribi, Salanne, and Chartrand 2016):

$$\kappa_i(T) = K_i k_B \left(\frac{N_A n_i}{V_i(T_{m,i})} \right) C_{0,i} \left(1 - \alpha_i(T_{m,i}) \left(\gamma_i(T_{m,i}) + \frac{1}{3} \right) (T - T_{m,i}) \right), \tag{10}$$

where K_i is a material constant, k_B is the Boltzmann constant, N_A is Avogadro's number, n_i is the number of atoms in the compound, V_i is the molar volume, $C_{0,i}$ is the speed of sound, α_i is the thermal expansivity, γ_i is the Gruneisen parameter, and $T_{m,i}$ is the melting temperature. Note that $C_{0,i}$, α_i , V_i, and γ_i are all functions of temperature, and are evaluated at $T_{m,i}$ in Eq. (10). The Gruneisen parameter is evaluated at the melting point as:

$$\gamma_i(T_{m,i}) = \frac{M_i \alpha_i C_{0,i}(T_{m,i})}{C_{p,i}(T_{m,i})}, \tag{11}$$

where M_i is the molar mass, and $C_{p,i}$ is the heat capacity, which is also a function of temperature. Because of the manner in which Eq. (10) was derived (Gheribi, Torres, and Chartrand 2014), which is rooted in a

thermodynamic description of κ_i (Ross et al. 1984), the thermal expansivity takes on a somewhat peculiar form:

$$\alpha_i = \frac{\delta(\ln(\rho_i))}{\delta T}, \tag{12}$$

where ρ_i is the density. This expression assumes that α_i is evaluated as some specific pressure; however, the density of molten salt has not been evaluated as a function of pressure, so it will be assumed that α_i is independent of the small pressure range that may be anticipated in molten salt systems. In order to evaluate Eq. (12) at $T_{m,i}$, we can approximate it as:

$$\alpha_i(T_{m,i}) \approx \ln(\rho_i(T_{m,i} + 1)) - \ln(\rho_i(T_{m,i})). \tag{13}$$

In some cases, the experimental $C_{0,i}$ data are not available for certain compounds, but compressibility or bulk modulus data (oftentimes determined through molecular dynamics simulations) can be used to calculate $C_{0,i}$ via:

$$C_{0,i}(T_m) = \sqrt{\frac{1}{\beta_i \rho_i(T_{m,i})}}, \tag{14}$$

where β_i is the compressibility (which is the inverse of the bulk modulus), and ρ_i is the density of compound i.

With these parameters calculated for the compounds of a molten salt mixture which has a total of I constituents, the mixture's heat capacity, speed of sound, thermal expansion, and molar volume ($C_{p,mix}$, $C_{0,mix}$, α_{mix}, and V_{mix}) can be calculated at the melting point of the mixture $T_{m,mix}$ using the following mixing rules:

$$C_{p,mix}(T_{m,mix}) = \sum_{i=1}^{I} x_i C_{p,i}(T_{m,mix}), \tag{15}$$

$$C_{0,mix}(T_{m,mix}) = \sum_{i=1}^{I} x_i C_{0,i}(T_{m,mix}), \tag{16}$$

$$\alpha_{mix}(T_{m,mix}) = \sum_{i=1}^{I} \phi_i \alpha_i(T_{m,mix}), \tag{17}$$

$$V_{mix}(T_{m,mix}) = \sum_{i=1}^{I} \frac{x_i M_i}{\rho_i(T_{m,mix})}, \tag{18}$$

where x_i is the molar fraction, and ϕ_i is the volume fraction of compound i in the mixture. Note that Eq. (15) is the Neumann–Kopp rule of mixing which is frequently used for heat capacity of molten salt, Eq. (16) is analogous to Eq. (15), Eq. (17) was put forth by Gallagher et al. (Gallagher et al. 2022), and Eq. (18) is the rule of additive molar volumes. Note that $\alpha_{mix}(T_{m,mix})$ and $V_{mix}(T_{m,mix})$ can both be determined if the density as a function of temperature has been measured for the mixture in question, or if an RK model can

be generated to more accurately estimate the deviation from these ideal mixing assumptions. If not, then Eqs. (17) and (18) should be considered as part of the generalized model.

Now, with a manner by which $C_{p,mix}$, $C_{0,mix}$, α_{mix}, and V_{mix} can be readily calculated, the thermal conductivity of the mixture can be determined analogously to Eq. (10):

$$\kappa_{mix}(T) = K_{mix}k_B\left(\frac{N_A n_{mix}}{V_{mix}(T_{m,mix})}\right)C_{0,mix}(T_{m,mix})\left(1-\alpha_{mix}(T_{m,mix})\left(\gamma_{mix}(T_{m,mix})+\frac{1}{3}\right)(T-T_{m,mix})\right)(1-\delta_{mix}), \quad (19)$$

where K_{mix} is a material constant for the mixture, n_{mix} is the molar average of the number of ions per compound in the mixture, and δ_{mix} is a non-ideal mixing term which is intended to account for ionic mass differences between the constituents of the mixture (Gheribi and Chartrand 2016). This δ_{mix} term has been used extensively for mixtures of alkali and alkaline earth halide melts, as well as nitrate and carbonate mixtures (Gheribi and Chartrand 2016; Gheribi, Phan, and Chartrand 2022; Gallagher et al. 2022; Yang et al. 2023; Gheribi et al. 2024). This term can be defined by (Gallagher et al. 2022):

$$\delta_{mix}(T) = 0.4872\frac{\kappa_{mix,id}(T)}{k_B C_{0,mix}(T_{m,mix})(n_{mix} * N_A * (1/V_{mix}(T_{m,mix})))^{2/3}} * g_{mass}, \quad (20)$$

where $\kappa_{mix,id}$ is the ideal thermal conductivity of the mixture (i.e., the right-hand-side of Eq. (19) prior to the $(1-\delta_{mix}(T))$ term), and g_{mass} is a mass fluctuation term which is defined as

$$g_{mass} = \sum_{i=1}^{I} x_i\left(\frac{M_i}{M_{mix}} - 1\right)^2, \quad (21)$$

where M_{mix} is the average molar mass of the mixture.

However, there are a few reasons why the authors of this report believe that this term can be considered to be approximately equal to zero when extending this kinetic theory model to include actinide-bearing mixtures. Firstly, g_{mass} has been defined based on the assumption that the molten salt mixture is a random mixture of atoms, similar to ideal solid solutions (Gheribi et al. 2014; Abeles 1963); the validity of a solid solution model as applied to a molten salt is not entirely obvious, as the phonon scattering rate in molten salts may not be expected to act similarly as a function of ionic mass differences as for ideal solid solutions. In a solid solution, one assumes that there exists some perfect cubic lattice of the same atom, in which an atom of a different molecular weight replaces one of these atoms, creating anharmonicity that affects the phonon relaxation time (Klemens 1955). This mathematical treatment of anharmonicity may in fact break down when the medium is a liquid mixture with significant rates of ion self-diffusion, and the structure of the endmembers is already highly disordered. Additionally, this mass fluctuation term was formulated on the basis of atomic molar mass differences, whereas this was adapted to be based on compound molar mass differences (Gheribi, Salanne, and Chartrand 2016), for which the basis of such a decision is also unclear. Secondly, for the molten salt mixtures which have been studied in the context of a kinetic theory model with the inclusion of a mass fluctuation term (Gheribi and Chartrand 2016; Gheribi, Phan, and Chartrand 2022; Gallagher et al. 2022; Yang et al. 2023; Gheribi et al. 2024), the inclusion of a δ_{mix} generally results in negative deviations of thermal conductivity that are between 0–20% (except for LiF-KF which is substantially higher (Gheribi and Chartrand 2016)), and the uncertainty in the experimental data used to validate this model can commonly be larger than that, even when considering the comparatively

more consistent and reliable datasets. Therefore, it is difficult to draw the conclusion that δ_{mix} as defined in Eq. (20) makes the model obviously more accurate.

Finally, and most importantly, when actinide salts are in the mixture, the g_{mass} term can become significantly larger than for any of the molten salt mixtures such as those containing only halides, carbonates, or nitrates; this leads to unrealistically low estimates of $\kappa_{mix}(T)$, as will be shown in the next section. For all of these reasons, $\delta_{mix} \approx 0$ herein, and thus

$$\kappa_{mix}(T) \approx K_{mix} k_B \left(\frac{N_A n_{mix}}{V_{mix}(T_{m,mix})} \right) C_{0,mix}(T_{m,mix}) \left(1 - \alpha_{mix}(T_{m,mix}) \left(\gamma_{mix}(T_{m,mix}) + \frac{1}{3} \right) (T - T_{m,mix}) \right). \tag{22}$$

The next consideration is the definition of K_{mix}, which accounts for the degree of complexity in the melt. In order to put forth a more simplistic and thus more generalizable model, the more simple definition of K_{mix} put forth by Yang et al. (Yang et al. 2023) is employed:

$$K_{mix} = x_i K_i, \tag{23}$$

where

$$K_i = 1 + n_i^+ / n_i^-, \tag{24}$$

where n_i^+ / n_i^- is the ratio of cationic to anionic complexes in the i^{th} constituent of the mixture. It can be deduced from several molecular dynamics studies that alkali halides are dissociated (Walz and Van der Spoel 2021), whereas any compounds with anions of higher valences are expected to be polymers. Thus, assuming the anionic valency of the i^{th} constituent is defined as v_i, then:

$$n_i^+ / n_i^- = \begin{cases} 2, & v_i = 1 \\ 1, & v_i > 1 \end{cases}. \tag{25}$$

What this means for all actinide halides, which may be constituents in fuel salt mixtures for MSRs, is that their assumed n_i^+ / n_i^- is always 1, because they are either trivalent or tetravalent.

4.3 VALIDATION WITH EXPERIMENTAL DATA

A validation of the model described in the previous section was performed based on all experimental thermal conductivity data contained within MSTDB-TP v4.0 for mixtures. The validation does not include the pure compound data because for pure compounds, Eq. (19) reduces to Eq. (10) in those cases where Eq. (10) is already well validated (Gheribi, Torres, and Chartrand 2014). As such, there are really only a handful of experimental studies with which the model described by Eq. (22) can be compared for validation purposes (Bobrova, Dokutovich, and Mushnikov 2023; Merritt et al. 2022; Khokhlov et al. 2011; Termini et al. 2024; Rudenko et al. 2024; Xu et al. 2018; AV Rudenko et al. 2024; Wang et al. 2021; Rose et al. 2023). Figure 8 shows the comparison between the experimentally measured thermal conductivities of mixtures in MSTDB-TP and the output of the kinetic theory model described by Eq. (22 as a parity plot.

What is clear from Fig. 8 is that the kinetic theory model has no apparent bias between salt systems with or without actinides. One would expect that, if the δ_{mix} term were indeed significant, that the kinetic theory

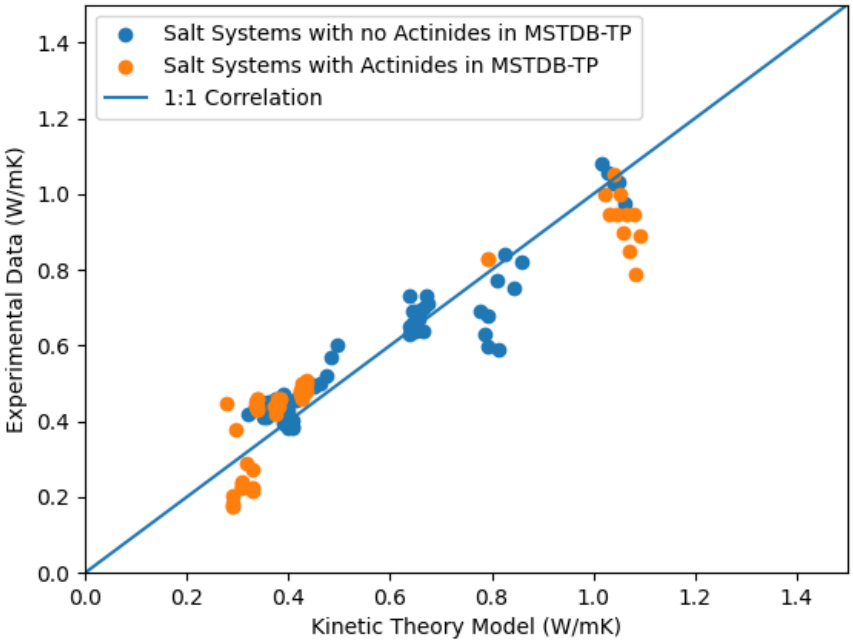

Figure 8. Parity plot showing the comparison between experimentally measured κ_{mix} values versus those determined by the kinetic theory model summarized by Eq. (22).

model would be over-predicting the thermal conductivity systematically for actinide-bearing mixtures. This would therefore place the data points in Fig. 8 systematically below the 1:1 correlation. Because this is not the case, this model validation in Fig. 8 suggests that the assumption of δ_{mix} being approximately equal to zero is indeed reasonable.

Another way to visualize the model validation is presented in Fig. 9, where the percent discrepancy between the model and the experimental data are plotted as a function of the average molar mass difference between the mixture constituents. In salt systems which bear actinides, the average molar mass difference tends to be quite high. Again, this plot showcases that there is no particular bias, such that the percent discrepancy between the model and the experiment does not obviously change as a function of average molar mass difference. Of course, it is important to recognize one feature of Fig. 9, which is that the percent discrepancy between the model and experiment tends to be more severe for actinide-bearing salt systems, as opposed to salts which do not bear any actinides. This may be due to a few different factors: (1) experimental error on actinide-bearing salt measurements may be higher due to their lower thermal conductivities and challenges with purity maintenance; (2) kinetic theory models of the actinide bearing mixtures (which are complex-forming) are more susceptible to error introduced due to the simplistic definition of K_{mix} in Eq. (23); (3) these models for actinide-bearing mixtures rely to a more significant extent on approximations to determine their speeds of sound, whereas the speeds of sound are better characterized for mixtures which do not bear actinides.

To analyze this kinetic theory model more closely, in the context of one particular actinide-bearing salt system, the LiF-BeF_2-UF_4 system is assessed in Fig. 10. The goal is to see how the kinetic theory model performs in comparison to measurements conducted by Bobrova, Dokutovich, and Mushnikov (2023), in which small amounts of UF_4 were added to LiF-BeF_2 in order to quantify the extent to which the thermal

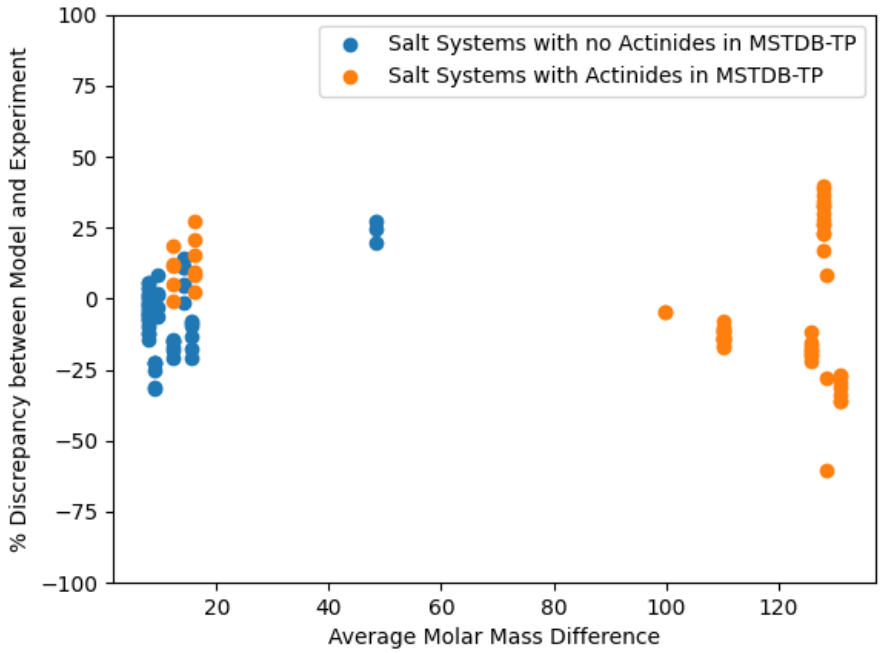

Figure 9. Percent difference between experimentally measured κ_{mix} values versus those determined by the kinetic theory model summarized by Eq. (22).

conductivity was altered. In addition, a handful of other experimental measurements (Kato et al. 1983; Cooke, Hoffman, and Keyes Jr. 1969; Redkin et al. 2022) of LiF-BeF_2 are captured in Fig. 10 to compare against the measurement of Bobrova. What is clear is that Bobrova's measurement indicates that small additions of UF_4 to LiF-BeF_2 result in a small decrease in thermal conductivity; this is consistent with the kinetic theory model, where $\delta_{mix} = 0$. In contrast, when a non-zero δ_{mix} is included in the model, the thermal conductivity plummets to non-physically low levels. This example case provides further evidence that the assumption of $\delta_{mix} = 0$ is reasonable, and that the formalism for a non-zero δ_{mix} as per Eq. (20) is, at the very least, over-approximating the effect of molar mass differences among mixtures in the thermal conductivity.

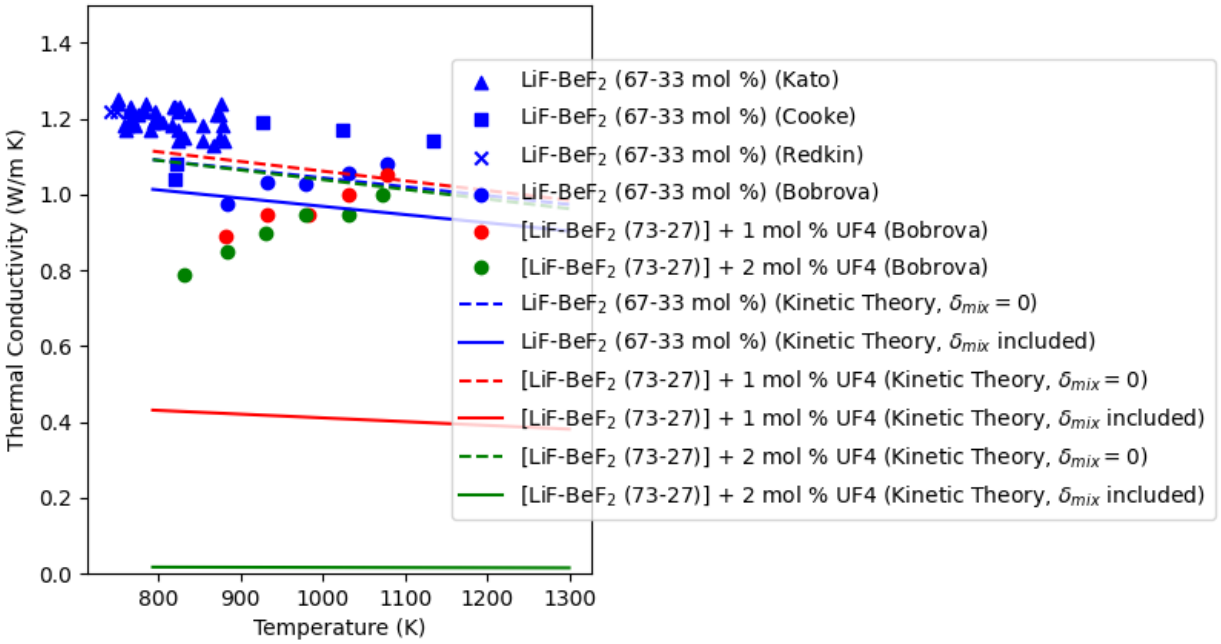

Figure 10. Measurements of κ_{mix} for select mixtures within the LiF-BeF_2-UF_4 system, in comparison with kinetic theory models. Two kinetic theory models have been plotted; one including the effect of $\delta_{mix}(T)$ as calculated based on Eq. (20), and one considering $\delta_{mix}(T)$ to be zero, as in Eq. (22).

5. FUTURE DEVELOPMENTAL EFFORTS

5.1 SURFACE TENSION PREDICTION

While surface tension (γ) of a particular system is characterized by Eq. (1), it is advantageous to incorporate component concentration terms for the development of a more comprehensive model for multicomponent systems. Several models have been historically proposed for the surface tension of multicomponent systems. A future effort toward MSTDB-TP development will consider these models through applications to existing datasets of multicomponent systems in MSTDB. These models include ideal mixing, non-ideal binary mixing, two models by Eberhart for binary and multicomponent systems, evaluation based on Pockels number, and other models developed by Brock and Bird, Butler, Goldsack and Sarvas, Hu, Li, Pandey, Dutcher, Kleinheins, and Sonawane.

5.1.1 Ideal & Non-ideal Mixing

The ideal mixing model assumes a simple linear contribution from each constituent to the surface tension of the system. This relationship is described by:

$$\gamma_{ideal} = \sum_i \gamma_i x_i, \tag{26}$$

where γ_i is the surface tension of each component and X_i is the molar fraction of each component.

The non-ideal binary mixing model introduces an additional parameter, $\Delta\gamma$, known as the excess surface tension to capture the deviation from ideality. The excess surface tension is based on a binary interaction parameter, C_1, determined through a least-squares fit. This expanded model is represented by:

$$\gamma_{non-ideal} = \gamma_1 x_1 + \gamma_2 x_2 + \Delta\gamma \qquad \Delta\gamma = C_1 x_1 x_2 (\gamma_1 - \gamma_2). \tag{27}$$

Further expansion of this non-ideal mixing model to n components is the basis of the RK formalism, detailed in Section 2.2:

$$\Delta\gamma_{RK} = \sum_{i=1}^{n} \sum_{j>i}^{n} x_i x_j \sum_{k=0}^{m-2} C_k^{ij} (x_i - x_j)^k \ , \tag{28}$$

where m is the maximum degree of polynomial fitting.

5.1.2 Brock-Bird Relation

Brock and Bird observed that the principle of corresponding states, developed by van der Waals, had not yet been fully examined for its application to various physical properties. The original form of this relation was found to be inadequate, likely due to unaccounted alignment effects at the interface which are highly sensitive to molecular shapes and interactions (Brock and Bird 1955). Modifications based on critical constants were proposed for the development of an improved correlation for multicomponent systems. The Brock-Bird correlation is given by (Reza Vakili-Nezhaad et al. 2019):

$$\begin{gathered} \gamma = \left(0.12103\left(1 + \frac{T_{brm} * \ln(P_{cm})}{1 - T_{brm}}\right) - 0.28\right) * P_{cm}^{2/3} * T_{cm}^{1/3} * \left(1 - \frac{T}{T_{cm}}\right)^{11/9} \\ T_{brm} = \sum_i x_i \frac{T_{bi}}{T_{ci}} \qquad P_{cm} = \sum_i x_i P_{ci} \qquad T_{cm} = \sum_i x_i T_{ci} \end{gathered} \ , \tag{29}$$

where T_{brm} is the reduced boiling temperature of the mixture, P_{cm} is the critical pressure of the mixture, T_{cm} is the critical temperature of the mixture, x_i is the mole fraction of component i, T_{bi} and T_{ci} are the boiling temperature and critical temperature of component i, and P_{ci} is the critical pressure of component i. The original authors suggested this correlation is best suited for simple inorganic substances and a wide variety of organic substances and that it may not hold for very light atoms/molecules, molten metals, highly polar inorganic substances (water, ammonia, acids), associating substances (alcohols, carboxylic acids), and fused salts (Brock and Bird 1955). Previous application of this relation to ternary hydrocarbon mixtures resulted in average percent deviation of 7.9% from experimental values (Reza Vakili-Nezhaad et al. 2019).

5.1.3 Butler Relation

The Butler relation was derived by J.A.V. Butler in a 1932 publication based on a thermodynamics approach (Butler 1932). This work was revisited in a 2021 publication by Santos and is summarized here (Soledade C. S. Santos and Reis 2021). The basis of this derivation is a planar surface phase of components A and B at fixed temperature T and pressure p that is in thermodynamic equilibrium with the liquid phase. The Gibbs energy of the surface phase is given by:

$$dG^s = -S^s dT + V^s dp + \gamma dA + \mu_A dn_A^s + \mu_B dn_B^s \tag{30}$$

where S is entropy, V is volume, γ is surface tension, A is surface area, μ_i is chemical potential of species i, and n_i is molar amount of species i. Superscript s denotes the surface phase, and applies only to properties whose equilibrium values are different in each phase. It then follows that:

$$\gamma = \left(\frac{\partial G^s}{\partial A}\right)_{T,p,n_A^s,n_B^s} \qquad \mu_B = \left(\frac{\partial G^s}{\partial n_B^s}\right)_{T,p,A,n_A^s} . \tag{31}$$

Partial differentiation of the μ_B equation above gives:

$$\left(\frac{\partial G^s}{\partial n_B^s}\right)_{T,p,n_A^s} = \left(\frac{\partial G^s}{\partial n_B^s}\right)_{T,p,A,n_A^s} + \left(\frac{\partial A}{\partial n_B^s}\right)_{T,p,n_A^s} \left(\frac{\partial G^s}{\partial A}\right)_{T,p,n_A^s,n_B^s} , \tag{32}$$

where the partial derivative of surface area with respect to the molar amount of species B at the surface, $(\partial A/\partial n_B^s)_{T,p,n_A^s}$, is equal to the partial molar surface area of B at constant temperature and pressure and is designated as $\overline{A_B}(T,p)$. Therefore, by substituting this term and Eq. (31) into Eq. (32), a classical thermodynamics derivation is obtained for chemical potential in terms of surface tension, given by:

$$\mu_B = \left(\frac{\partial G^s}{\partial n_B^s}\right)_{T,p,n_A^s} - \gamma \overline{A_B}(T,p) . \tag{33}$$

To simplify terms, the notation g_B^s is introduced for the partial derivative $(\partial G^s/\partial n_B^s)_{T,p,n_A^s}$. In the bulk phase, the chemical potential of species B (μ_B) is described by:

$$\mu_B = \mu_B^* + RT\ln(\alpha_B x_B) , \tag{34}$$

where R is the universal gas constant, α_B is the activity coefficient of species B at mole fraction x_B, and the asterisk denotes the pure-component property. Accordingly, the standard state is pure liquid B.

The equilibrium condition of surface and bulk phases requires uniformity of the chemical potential, μ_B, such that:

$$g_B^s = \mu_B^* + \mu\overline{A_B}(T,p) + RT\ln(\alpha_B x_B) , \tag{35}$$

which is valid over the full compositional range. Since $\alpha_B = 1$ for $x_B = 1$, then:

$$g_B^{*,s} = \mu_B^* + \gamma_B^* A_B^* \quad . \tag{36}$$

Because $g_B = (\partial G/\partial n_B)_{T,p,n_A} = \mu_B$, consequently the partial derivative $g_B^{*,s}$ at the surface is not equal to the bulk property $g_B^* = \mu_B^*$. Subtracting Eq. (36) from Eq. (35) yields the following:

$$g_B^s = g_B^{*,s} - \gamma_B^* A_B^* + \gamma \overline{A_B}(T,p) + RT\ln(\alpha_B x_B) \quad , \tag{37}$$

$$\gamma = \gamma_B^* \frac{A_B^*}{\overline{A_B}(T,p)} + \frac{g_B^s - g_B^{*,s}}{\overline{A_B}(T,p)} - \frac{RT}{\overline{A_B}(T,p)} \ln(\alpha_B x_B) \quad . \tag{38}$$

Only well-established chemical and phase-equilibria thermodynamics are utilized in transforming Eq. (33) into Eq. (38), which is therefore a rigorous expression for surface tension in terms of mixture composition at constant T and p, excluding any additional thermodynamic approximations or assumptions.

Butler's objective was to establish an equation for the difference $g_B^s - g_B^{*,s}$. Expressing this difference in the form of Eq. (34) to account for changes in composition at fixed T and p, Butler proposed:

$$g_B^s = g_B^{0,s} + RT\ln(\alpha_B^s x_B^s) \quad , \tag{39}$$

where $g_B^{0,s}$ is the corresponding standard-state property. Combining equations 33, 34, and 39 yields:

$$\mu_B = g_B^{0,s} - \gamma \overline{A_B}(T,p) + RT\ln(\alpha_B^s x_B^s) \quad . \tag{40}$$

Expanding this equation by incorporating the balance of $g_B^{0,s} = g_B^{*,s} + g_B^{0,s} - g_B^{*,s}$ and involving Eq. (36) yields:

$$\mu_B = \mu_B^* + g_B^{0,s} - g_B^{*,s} - \gamma \overline{A_B}(T,p) + \gamma_B^* A_B^* + RT\ln(\alpha_B^s x_B^s) \quad . \tag{41}$$

This approach implicitly assumes a standard chemical potential at the surface ($\mu_B^{0,s}$) with the form:

$$\mu_B^{0,s} = \mu_B^* + g_B^{0,s} - g_B^{*,s} - \gamma \overline{A_B}(T,p) + \gamma_B^* A_B^* \quad . \tag{42}$$

However, Butler considers a constant $g_B^{0,s}$ independent of surface-phase composition and therefore equal to $g_B^{*,s}$. Thus, from Eqs. (38) and (39) one obtains the commonly accepted form of the Butler equation, given by:

$$\gamma = \gamma_B^* \frac{A_B^*}{\overline{A_B}(T,p)} + \frac{RT}{\overline{A_B}(T,p)} \ln\left(\frac{\alpha_B^s x_B^s}{\alpha_B x_B}\right) \quad , \tag{43}$$

and Butler's standard chemical potential becomes:

$$\mu_B^{0,s}(\text{Butler}) = \mu_B^* - \gamma \overline{A_B}(T,P) + \gamma_B^* A_B^* \quad . \tag{44}$$

5.1.4 Dutcher Relation

The relation developed by Dutcher predicts surface tension of aqueous electrolyte solutions ranging from infinite dilution to molten salt. This derivation involves the ion valency and radius, melting temperature, and molar volume, and explores the effect of salt-salt interactions (Dutcher, Wexler, and Clegg 2010).

Beginning with salt species dissolved in water, the surface tension (γ_{mix}) can be expressed by component mole fractions (x_i) and pure component surface tension (γ_i) (Dutcher, Wexler, and Clegg 2010):

$$\ln(\gamma_{mix}) = x_w \ln(\gamma_w) + x_s \ln(\gamma_s) \quad , \tag{45}$$

where subscripts w and s refer to water and salt, respectively. This relation was moderately successful for representing surface tensions of highly soluble salts such as nitrates. For less soluble species such as chlorides, Eq. (45) only holds for very dilute concentrations (Dutcher, Wexler, and Clegg 2010).

This limitation was addressed by correlating the behavior with dilute concentrations of water in concentrated salt. At low salt concentrations, salt ions are solvated by hydration shells formed around the ion, and the temperature dependence of the surface tension is represented by:

$$\gamma = \gamma_w + x_s F_{ws}(T) \qquad F_{ws}(T) = a_{ws} + b_{ws} T \quad , \tag{46}$$

where $F_{ws}(T)$ is a linear function representing the interaction of salt and water, and contains two fitted parameters, a_{ws} and b_{ws}. A similar relationship is put forth for the case of a predominantly salt system where water is solvated by a salt structure formed around the water molecules, represented by:

$$\gamma = \gamma_s + x_w F_{sw}(T) \qquad F_{sw}(T) = a_{sw} + b_{sw} T \quad , \tag{47}$$

and noting that $a_{sw} \neq a_{ws}$ and $b_{sw} \neq b_{ws}$ (Dutcher, Wexler, and Clegg 2010). Through Eq. (45), these expressions can be combined to obtain a single expression encompassing the full compositional range:

$$\ln(\gamma_{mix}(T)) = x_w \ln(\gamma_w(T) + x_s F_{ws}(T)) + x_s \ln(\gamma_s(T) + x_w F_{ws}(T)) \quad . \tag{48}$$

Extending Eq. (48) to a mixture of molten salts, s_1 and s_2, yields:

$$\ln(\gamma_{mix}(T)) = x_{s_1} \ln(\gamma_{s_1}(T) + x_{s_2} F_{s_1,s_2}(T)) + x_{s_2} \ln(\gamma_{s_2}(T) + x_{s_1} F_{s_2,s_1}(T)) \quad , \tag{49}$$

where γ_{s_1} and γ_{s_2} are the surface tensions of the two pure molten salts, while F_{s_1,s_2} and F_{s_2,s_1} represent the salt–salt interaction functions containing fitted parameters a_{s_1,s_2}, b_{s_1,s_2}, a_{s_2,s_1}, and b_{s_2,s_1}. Generalizing this equation to mixtures containing N components which may include water yields:

$$\ln[\gamma_{mix}(T)] = \sum_i^N x_i \ln\left(\gamma_i(T) + \sum_j^N x_j F_{ij}(T)\right) \quad , \tag{50}$$

where $j \neq i$ and the interaction function $F_{ij}(T)$ is given by:

$$F_{ij}(T) = a_{ij} + b_{ij}(T) \quad , \tag{51}$$

where a_{ij} and b_{ij} are fitted parameters.

5.1.5 Eberhart Binary and Multicomponent Relations

A model for the surface tension of binary liquid mixtures was derived in 1966 by Eberhart (Eberhart 1966). This model operates on three assumptions (Kleinheins et al. 2024):

(1) The surface tension of a mixture (γ_{mix}) is the average of the pure component surface tensions (γ_i) weighted by the surface mole fractions (x_i^s):

$$\gamma_{mix} = \gamma_1 x_1^s + \gamma_2 x_2^s \tag{52}$$

(2) Absorption and desorption of substances from the surface is described by a distribution constant at equilibrium, $K_i = a_i^s / a_i$, where a_i^s is the surface activity and a_i is the bulk activity of substance i. The separation factor is defined by:

$$S_{12} = K_2 / K_1 \quad . \tag{53}$$

(3) Ideal mixing occurs in the bulk and at the surface, resulting in:

$$a_i = x_i \qquad a_i^s = x_i^s \quad , \tag{54}$$

where x_i is the bulk mole fraction of substance i. The resulting model for binary mixtures is therefore given by:

$$\gamma_{mix} = \frac{\gamma_1 x_1 + \gamma_2 S_{12} x_2}{x_1 + S_{12} x_2} \quad , \tag{55}$$

where S_{12} is an experimentally determined fitting parameter with the property $S_{12} * S_{21} = 1$. Thus, setting $S_{12} = S_{21} = 1$ leads to the simple ideal mixing relation of $\gamma_{mix} = \gamma_1 x_1 + \gamma_2 x_2$.

Furthermore, Kleinheins derived a Sigmoid model for binary systems given by:

$$\gamma_{mix} = \gamma_1 - (\gamma_1 - \gamma_2)(10^{pd} + 1)\frac{x_2^d}{10^{pd} + x_2^d} \quad , \tag{56}$$

where the fitted parameter p relates to the inflection point in surface tension on a logarithmic x_2-axis and the other fitted parameter d relates to the slope at that point (Kleinheins et al. 2023). In the case of $d = 1$, the Sigmoid model reduces to the Eberhart model with the relation $10^p = (S_{12} - 1)^{-1}$. Consequently, the Eberhart model produces sigmoidal surface tension curves on a logarithmic x_2-axis with an inflection point at $x_2 = (S_{12} - 1)^{-1}$ (Kleinheins et al. 2024).

The ideal multicomponent Eberhart model is a simplified case of the Connors-Wright model where $a_{ij} = b_{ij} = 1 - 1/S_{ij}$ with a_{ij} and b_{ij} as fitted parameters from the Connors-Wright model (Kleinheins et al. 2023; Shardt and Elliott 2017). The Connors-Wright model is equivalent to the Chunxi model which is based on a Gibbs free energy expression of bulk and surface phases (Chunxi, Wenchuan, and Zihao 2000). The multicomponent Eberhart model is given by:

$$\gamma_{mix} = \sum_{i=1}^{n} \gamma_i x_i + \sum_{i=1}^{n} \left(\frac{x_i}{\sum_{j=1}^{n} x_j / S_{ji}} \sum_{j=1}^{n} \frac{x_j}{S_{ji}} (\gamma_j - \gamma_i) \right) \quad , \tag{57}$$

with the properties $S_{ii} = 1$ and $S_{ji} = 1/S_{ij}$. The first summation over i in this model corresponds to a simple ideal mixing model, while the second summation over i accounts for binary interactions (Kleinheins et al. 2024). For a 2-component mixture, Eq. (57) reduces to Eq. (55). For a 3-component mixture, this model results in:

$$\begin{aligned} \gamma_{mix} = {} & \gamma_1 x_1 + \gamma_2 x_2 + \gamma_3 x_3 \\ & + x_1 x_2 (\gamma_1 - \gamma_2) \left(\frac{-S_{12}}{x_1 + x_2 S_{12} + x_3 S_{13}} + \frac{S_{21}}{x_1 S_{21} + x_2 + x_3 S_{23}} \right) \\ & + x_1 x_3 (\gamma_1 - \gamma_3) \left(\frac{-S_{13}}{x_1 + x_2 S_{12} + x_3 S_{13}} + \frac{S_{31}}{x_1 S_{31} + x_2 S_{32} + x_3} \right) \\ & + x_2 x_3 (\gamma_2 - \gamma_3) \left(\frac{-S_{23}}{x_1 S_{21} + x_2 + x_3 S_{23}} + \frac{S_{32}}{x_1 S_{31} + x_2 S_{32} + x_3} \right) \end{aligned} \quad . \tag{58}$$

In the case of a binary system ($x_3 = 0$), Eq. (58) reduces to Eq. (55). This model is applicable to any system composed of water, salts, organics, and/or amphiphilic substances (Kleinheins et al. 2024).

5.1.6 Goldsack-Sarvas Relation

The Goldsack-Sarvas method has been applied to several polar–polar, non-polar–non-polar, and polar–non-polar systems with good success, reporting average errors less than 1% for a variety of systems assuming ideal chemical potential equations and molar surface areas calculated from bulk density values (Goldsack and Sarvas 1981). The authors suggest this equation holds for systems with surface tension differences $\leq$ 20 erg/cm^2. Systems with larger surface tension differences require the inclusion of activity coefficient effects (Goldsack and Sarvas 1981). This method is defined by:

$$\gamma = -\frac{RT}{A}\ln\left(\sum_i x_i \exp\left(-\frac{\gamma_i A}{RT}\right)\right) \qquad A = \pi\left(\frac{3}{4\pi}\right)^{2/3} N_A^{1/3} V^{2/3} \approx (1.02 * 10^8)\sum_i x_i V_i^{2/3} \quad , \tag{59}$$

where N_A is Avogadro's number, V is molar volume, x_i is component mole fraction, and A is molar surface area. This expression for A allows the implementation of the Butler equation under the assumptions that the surface phase is a monolayer, the molecules of each component can be approximated as spheres, the cross-sectional area of each molecule is the appropriate geometrical area presented at the surface, and the bulk density and surface density of component i are equal (Goldsack and Sarvas 1981). The latter assumption is likely not valid in general, but is useful for a first approximation because it enables the calculation of surface tension for mixtures based on known bulk properties of each component (Conway 1976).

For binary systems with large polarity differences, expansion of the logarithmic expression is required to derive an explicit expression in terms of the bulk system parameters. The Goldsack-Sarvas method details this expanded derivation for three different cases (Goldsack and Sarvas 1981). Each of these cases utilize the volume fraction (ϕ) defined by:

$$\phi_1 = \frac{X_1 V_1}{X_1 V_1 + X_2 V_2} \qquad \phi_2 = \frac{X_2 V_2}{X_1 V_1 + X_2 V_2} \quad . \tag{60}$$

Now defining terms $B_1 = \exp((\gamma - \gamma_1)(A_1/RT))$ and $B_2 = \exp((\gamma - \gamma_2)(A_2/RT))$ allows the derivation of an explicit relation for surface tension in terms of bulk parameters, given by:

$$\phi_1 B_1\left[1 + \phi_2\left(1 - \frac{V_1}{V_2}\right)\right] + \phi_2 B_2\left[1 + \phi_1\left(1 - \frac{V_2}{V_1}\right)\right] - \phi_1\phi_2 B_1 B_2\left[\left(1 - \frac{V_1}{V_2}\right) + \left(1 - \frac{V_2}{V_1}\right)\right] = 1 \quad . \tag{61}$$

For systems where $(1 - V_1/V_2)$ is in the range of 0.1–0.2 and approximately equal to $(V_2/V_1 - 1)$, which is the case for most organic systems, the last term in Eq. (61) is significantly smaller than the first two terms and may be neglected, yielding:

$$B_1\left[\phi_1 + \phi_1\phi_2\left(1 - \frac{V_1}{V_2}\right)\right] + B_2\left[\phi_2 + \phi_1\phi_2\left(1 - \frac{V_2}{V_1}\right)\right] = 1 \quad . \tag{62}$$

In this equation, the terms $\phi_1\phi_2(1 - V_1/V_2)$ and $\phi_1\phi_2(1 - V_2/V_1)$ are on the order of 0.025. Neglecting these terms as a further approximation and replacing B_1 and B_2 with their definitions yields:

$$\phi_1 \exp\left[(\gamma - \gamma_1)\frac{A_1}{RT}\right] + \phi_2 \exp\left[(\gamma - \gamma_2)\frac{A_2}{RT}\right] = 1 \quad . \tag{63}$$

The following equations are the implicit forms of the previous three equations and can be applied for systems violating the small surface tension difference requirement. By using an approximate value on the volume fraction scale for γ on the right side of each equation, denoted by γ', an explicit function can be defined.

The resulting explicit form solutions for binary system surface tensions based on Eqs. (61)–(63), respectively, are given by Eqs. (64)–(66). These equations are applicable to systems where component surface

tensions differ by > 10 dyn/cm and made explicit by using an approximate volume fraction scale value (γ') on the right-hand side.

$$\gamma = \gamma_1 - \frac{RT}{A_1}\left(\ln\left(1 + \phi_2\left(\exp\left[\frac{\gamma'(A_2 - A_1)}{RT}\right]\exp\left[\frac{\gamma_1 A_1 - \gamma_2 A_2}{RT}\right] - 1\right)\right)\right) \tag{64}$$

$$\gamma = \gamma_1 - \frac{RT}{A_1}\left(\ln\left(\phi_1\left[1 + \phi_2\left(1 - \frac{V_1}{V_2}\right)\right] + \phi_2\left[1 + \phi_1\left(1 - \frac{V_2}{V_1}\right)\right]\exp\left[\frac{\gamma'(A_2 - A_1)}{RT}\right]\exp\left[\frac{\gamma_1 A_1 - \gamma_2 A_2}{RT}\right]\right)\right) \tag{65}$$

$$\begin{aligned}\gamma = \gamma_1 - \frac{RT}{A_1}\Bigg(\ln\Bigg(\phi_1\left[1 + \phi_2\left(1 - \frac{V_1}{V_2}\right)\right] + \phi_2\left[1 + \phi_1\left(1 - \frac{V_2}{V_1}\right)\right]\exp\left[\frac{\gamma'(A_2 - A_1)}{RT}\right]\exp\left[\frac{\gamma_1 A_1 - \gamma_2 A_2}{RT}\right] \\ - \phi_1\phi_2\left[\left(1 - \frac{V_1}{V_2}\right) + \left(1 - \frac{V_2}{V_1}\right)\right]\exp\left[(\gamma' - \gamma_2)\frac{A_2}{RT}\right]\Bigg)\Bigg)\end{aligned} \quad . \tag{66}$$

5.1.7 Hu Relation

Hu proposed a new prediction model in 1997 that involves surface chemical potential and the Peng-Robinson equation of state (Hu et al. 1997). When applied to 73 binary systems and 8 ternary systems, this model resulted in average relative deviations of 1.35% and 3.52%, respectively. This model assumes uniform composition of the surface layer with different intermolecular interactions resulting in different properties from the bulk and vapor phases. Following the prescription of chemical potential in the bulk liquid phase, the chemical potential for a component i in the surface phase of a mixture is given by:

$$\mu_{iS}^{M} = \mu_{iS}^{0} + RT\ln(f_{iS}^{M}) \quad , \tag{67}$$

where S denotes the surface layer, M denotes the mixture property, and f represents fugacity (Hu et al. 1997). While the bulk and surface phases are in equilibrium, the chemical potentials of component i are not identical in each phase because of surface tension in the surface phase. The difference in chemical potentials is represented by:

$$\begin{aligned}\gamma^{M}\overline{A_i^{M}} &= \mu_{iS}^{M} - \mu_{iB}^{M} = (\mu_{iS}^{0} - \mu_{iB}^{0}) + RT\ln(f_{iS}^{M}/f_{iB}^{M}) \\ \gamma A_i &= \mu_{iS} - \mu_{iB} = (\mu_{iS}^{0} - \mu_{iB}^{0}) + RT\ln(f_{iS}/f_{iB})\end{aligned} \quad . \tag{68}$$

Combining equations yields:

$$\gamma^{M}\overline{A_i^{M}} - \gamma A_i = RT\ln\frac{(f_{iS}^{M}/f_{iS})}{(f_{iB}^{M}/f_{iB})} \quad . \tag{69}$$

Substituting the fugacity coefficient ($f = P\phi$) in Eq. (69) and solving for mixture surface tension yields:

$$\gamma^{M} = \frac{A_i}{\overline{A_i^{M}}}\gamma_i + \frac{RT}{\overline{A_i^{M}}}\ln\frac{(P_s\phi_{iS}^{M}x_{iS}/P_{iS}\phi_{iS})}{(P_B\phi_{iB}^{M}x_{iB}/P_{iB}\phi_{iB})} \quad . \tag{70}$$

The use of Eq. (70) requires the following assumptions:

(1) The partial molar surface area ($\overline{A_i^{M}}$) in the mixture is the same as the pure liquid, calculated from:

$$\overline{A_i^{M}} = A_i = V_{iB}^{2/3}N_A^{1/3} \quad , \tag{71}$$

where V_{iB} is the molar volume of pure component i in the bulk.

(2) Fugacity coefficients ($\phi_{iS}^{M}, \phi_{iB}^{M}$) and pressures ($P_S, P_B$) of the surface and bulk phases can be calculated according to the Peng-Robinson equation of state (Peng and Robinson 1976):

$$P = \frac{RT}{V-b} - \frac{a(T)}{V(V+b)+b(V-b)} \quad , \tag{72}$$

where:

$$\begin{aligned} &a(T) = a(T_c) * \alpha(\omega, T) \\ &a(T_c) = 0.45724 * R^2 T_c^2 / P_c \\ &\alpha(\omega, T) = [1 + \alpha_\omega (1 - \sqrt{T/T_c})]^2 \\ &\alpha_\omega = 0.37464 + 1.54226\omega - 0.26992\omega^2 \\ &b = 0.07780 * RT/P_c \end{aligned} \quad . \tag{73}$$

In the above equations, a is a measure of the intermolecular attraction force in the van der Waals equation, α is a dimensionless function of reduced temperature and acentric factor and equals unity at the critical temperature, ω is the acentric factor, R is the universal gas constant, T_c and P_c are the critical temperature and critical pressure, respectively, and b represents the effective volume occupied by the gas molecules in the van der Waals equation.

(3) The following mixing rules apply to the surface and bulk phases (Hu 1983; Peng and Robinson 1976):

$$\begin{aligned} a_M &= \sum_{i=1}^{N} \sum_{j=1}^{N} x_i x_j a_{ij} \\ a_{ij} &= (1 - k_{ij}) \sqrt{a_{ii} a_{jj}} \\ b_M &= \sum_{i=1}^{N} x_i b_i \end{aligned} \quad , \tag{74}$$

where the subscript M denotes a mixture property, and k_{ij} is an adjustable parameter relating surface tensions of binary systems. The fugacity coefficient of component i in a mixture is calculated according to:

$$\ln(\phi_i^M) = \frac{b_i}{b_M}(z-1) - \ln(z-b) - \frac{A}{2B\sqrt{2}} \left(\frac{2\sum_{j=1}^{N} x_j a_{ij}}{a_M} - \frac{b_i}{b_M} \right) \ln \left(\frac{z + (1+\sqrt{2})B}{z + (1-\sqrt{2})B} \right) \quad , \tag{75}$$

where:

$$\begin{aligned} A &= a_M P / RT^2 \\ B &= b_M P / RT \\ z &= PV/RT \end{aligned} \quad . \tag{76}$$

Thus, Eq. (75) is used in calculating ϕ_{iS}^{M} and ϕ_{iB}^{M} by using x_{iS} and x_{iB}, respectively (Hu et al. 1997). Based on these assumptions, the resulting equation for mixture surface tension is given by:

$$\begin{aligned} \gamma^M &= \gamma_i + \frac{RT}{A_i} \ln \left(\frac{P_S x_{iS} \phi_{iS}^M}{P_B x_{iB} \phi_{iB}^M} \right) \qquad (i = 1, 2, ..., N) \\ &\sum_{i=1}^{N} x_{iS} = 1 \end{aligned} \quad . \tag{77}$$

5.1.8 Kleinheins Relation

In an effort to extend and improve the models put forth by Eberhart, Kleinheins considered the effects of surface and bulk non-ideality and partitioning synergism. Bulk non-ideality refers to interactions in the bulk that cause deviations from Raoult's law and are typically represented by activity coefficients. In other words, the solute-solute interactions may be stronger or weaker than solute-solvent interactions, which affects the adsorption-desorption equilibrium and changes the surface partitioning. Surface non-ideality, described by Fainerman, is a phenomenon where solute molecules at the surface may reorient or change packing behavior depending on the composition (Fainerman, Miller, and Aksenenko 2002). Partitioning synergism refers to the phenomenon where a mixture requires a lower solute concentration than any of the pure components do in order to reach a certain decrease in surface tension (Hua and Rosen 1982). An example of partitioning synergism caused by bulk non-ideality is the mixture of a salt and organic substance. In a phenomenon known as "salting out" the organic substance partitions more readily to the surface, and the surface tension is decreased at lower solute concentration of the organic substance than without the salt (Kleinheins et al. 2024). Partitioning synergism is also observed in systems with two surfactants, where enhanced partitioning of surfactant molecules may be driven by processes at the surface where surfactant concentration is higher than the bulk, rather than by bulk phase non-ideality alone (Kleinheins et al. 2024). Similarly, surface synergism describes a circumstance where a mixture has a lower surface tension than any of its pure components, and can be considered an extreme case of surface non-ideality (Kleinheins et al. 2024).

These phenomena, which are particularly applicable to molten salt systems, violate the assumptions forming the basis of the Eberhart models. Thus, the Kleinheins model attempts to reconcile this behavior by incorporating terms which capture the effects of non-ideality and synergism. First, the partitioning of less polar co-solutes (i) is influenced by the concentration of the salt (x_j), described by the following simple linear equation:

$$S_{1i}^{\text{non-ideal}} = S_{1i}(1 + x_j B_{ij}^{SO}) \quad , \tag{78}$$

where B_{ij}^{SO} is the bulk non-ideality factor for a system that is salting-out, containing a solute i mixed with a salt j. This $S_{1i}^{\text{non-ideal}}$ term replaces S_{1i} in Eqs. (57) and (58) for the case of non-ideal mixtures. A requirement for satisfying $S_{1i}^{\text{non-ideal}} > 0$ is that $B_{ij}^{SO} > -1$. Higher values of B_{ij}^{SO} indicate stronger salting-out, while $B_{ij}^{SO} = 0$ indicates this phenomena does not occur, and $-1 < B_{ij}^{SO} < 0$ indicates salting-in behavior (Kleinheins et al. 2024).

Experimental data has also shown that the presence of salts leads to surface non-ideality and slight surface synergism. In such systems, the critical micelle concentration (CMC), or the point at which the surface reaches its maximum coverage in surfactant molecules, is shifted to lower concentrations (partitioning synergism) and a lower surface tension can be reached at the CMC due to orientation/packing changes of the surfactant molecules at this surface (El Haber et al. 2023). This perturbation in surface tension can be modeled analogously to Eq. (78) by incorporating a function of salt concentration and a fit parameter via:

$$\gamma_i^{\text{non-ideal}} = \gamma_i(1 - x_j A_{ij}^{SO}) \quad , \tag{79}$$

where A_{ij}^{SO} is the surface non-ideality factor for a salting-out system containing a solute i mixed with a salt j (El Haber et al. 2023).

For a system with multiple surfactants partitioning to the surface, this may result in synergistic or antagonistic surface non-ideality, and mixed micelles start to form in the bulk (Kleinheins et al. 2024). This is distinct from salting-out (SO) non-ideality, and represented by mixed-micelle (MM) non-ideality. This phenomena is modeled by perturbing S_{1i}, S_{1j}, γ_i, and γ_j as a function of composition of the MM-forming

solutes i and j. It is assumed that the largest perturbation occurs when the fraction (x_{ij}^{MM}) of paired surfactant molecules is maximized, i.e., $x_i = x_j$.

$$x_{ij}^{MM} = 1 - \left| \frac{x_i - x_j}{x_i + x_j} \right| \quad . \tag{80}$$

This definition of x^{MM} implies that the degree of non-ideality scales with the relative solute ratio rather than dilution in the solvent (Kleinheins et al. 2024). The bulk non-ideality and partitioning synergism of mixed-micelle systems can be modeled analogously to Eqs. (78) and (79):

$$S_{1i}^{\text{non-ideal}} = S_{1i}(1 + x_{ij}^{MM} B_{ij}^{MM}) \qquad S_{1j}^{\text{non-ideal}} = S_{1j}(1 + x_{ij}^{MM} B_{ij}^{MM}) \quad , \tag{81}$$

where B_{ij}^{MM} is the bulk non-ideality factor for two MM-forming substance, i and j, with the requirement $B_{ij}^{MM} > -1$. The surface analogue for non-ideality and surface synergism of MM-forming systems is given by:

$$\gamma_i^{\text{non-ideal}} = \gamma_i(1 - x_{ij}^{MM} A_{ij}^{MM}) \qquad \gamma_j^{\text{non-ideal}} = \gamma_j(1 - x_{ij}^{MM} A_{ij}^{MM}) \quad , \tag{82}$$

where A_{ij}^{MM} is the surface non-ideality factor for two MM-forming substances, i and j (Kleinheins et al. 2024). Regarding the non-ideality in both salting-out and mixed-micelle systems, $A_{ij} > 0$ and $B_{ij} > 0$ represent synergistic non-ideality, while $A_{ij} < 0$ and $B_{ij} < 0$ represent antagonistic non-ideality. For systems involving more than two solutes, each pairwise solute-solute interaction should be considered following these equations.

To calculate non-ideal multicomponent surface tension according to Eqs. (78) and 79, one requires the mole fractions (x_i) and pure component surface tensions (γ_i) for each mixture component. Additionally, separation factors (S_{ij}) for each pairwise component combination are required, noting that a linear relationship between surface tension and component mole fraction results in $S_{ij} = 1$. Finally, surface and bulk non-ideality factors A_{ij} and B_{ij}, respectively, are required for each pairwise component combination, noting that ideal mixing behavior with the absence of synergism results in $A_{ij} = B_{ij} = 0$ (Kleinheins et al. 2024).

5.1.9 Li Relation

Li proposed a surface tension model for liquid mixtures originally based on the Wilson equation to represent excess Gibbs energy (Li, Wang, and Wang 2000) and later modified to use the non-random two liquid (NRTL) equation (Li and Wang 2001).

Beginning with the Wilson equation derivation, the molar Gibbs free energy (g) for a multicomponent liquid mixture at temperature T and pressure P is expressed by:

$$g(T,P) = \sum_i x_i(g_i^0(T,P) + RT\ln(x_i)) + g^{\text{ex}} \quad , \tag{83}$$

where x_i is mole fraction and $g_i^0(T,P)$ is the molar Gibbs free energy of component i at system temperature and pressure. Incorporating the Wilson equation to represent the molar excess Gibbs free energy (g^{ex}) yields:

$$\begin{gathered} g(T,P) = \sum_i x_i[g_i^0(T,P) + RT\ln(x_i)] - RT\sum_i x_i \ln\left(\sum_j x_j \Lambda_{ij}\right) \quad , \\ \Lambda_{ij} = \frac{v_j}{v_i}\exp\left(-\frac{U_{ij} - U_{ii}}{RT}\right) \end{gathered} \tag{84}$$

where v_i is the molar volume of component i and $U_{ij} - U_{ii}$ is the difference in interaction energy between molecular pair ij and ii (Li, Wang, and Wang 2000). Surface tension is defined via thermodynamics as the Gibbs energy required for an increase of unit surface area at constant temperature, pressure, and composition (i.e., per mole for total Gibbs energy (G), and per mole fraction for molar Gibbs energy (g)), given by:

$$\gamma = \left(\frac{\partial G^{(s)}}{\partial A}\right)_{T,P,\{n_i\}} = \left(\frac{\partial g^{(s)}}{\partial A}\right)_{T,P,\{x_i\}} \quad , \tag{85}$$

where superscript (s) denotes the surface phase, and $G^{(s)}$ and $g^{(s)}$ are related via $G^{(s)} = n^{(s)}_{\text{total}} g^{(s)}$.

Because the surface phase is several molecular layers thick and little is known a priori about surface phase composition and properties, it is assumed that concentration and Gibbs energy in the surface phase are proportional to those in the bulk phase, and Eq. (84) is an appropriate representation of Gibbs energy in the surface phase. This approximation can be adapted through adjustable parameters for a binary system. Substituting $g(T, P)$ in Eq. (84) for $g^{(s)}$ in Eq. (85) and incorporating a derivative manipulation on $g^{(s)}$ with respect to surface area yields an expression for the surface tension of a liquid mixture (γ_M):

$$\begin{aligned} \gamma_M &= \sum_i x_i \gamma_i - RT \sum_i \frac{x_i}{\sum_j x_j \Lambda_{ij}} \sum_j x_j \left(\frac{\partial \Lambda_{ij}}{\partial A}\right)_{T,P,x} \\ \left(\frac{\partial \Lambda_{ij}}{\partial A}\right)_{T,P,x} &= -\frac{\Lambda_{ij}}{RT}\left(\frac{\partial (U_{ij} - U_{ii})}{\partial A}\right)_{T,P,x} \end{aligned} \quad , \tag{86}$$

where the surface tension of pure component i is defined by $\gamma_i = (\partial g_i^{0(s)}/\partial A)_{T,P}$. Eq. (86) is the final expression for mixture surface tension and adjustable parameters for a binary system include $U_{ij} - U_{ii}$ and $(\partial(U_{ij} - U_{ii})/\partial A)_{T,P,x}$. It is assumed in Eq. (86) that the ratio of molar volume for any two components is unity when calculating the $\Lambda_{i,j}$ parameter, therefore:

$$\Lambda_{ij} = \exp\left(-\frac{U_{ij} - U_{ii}}{RT}\right) \quad . \tag{87}$$

This can be physically interpreted by saying the effect of molecular size on the excess Gibbs energy is negligible compared to the difference in intermolecular energy (Li, Wang, and Wang 2000).

Equation 86 is composed of two terms. The first is the pure-component contribution and the second is the excess surface tension arising from the cross-interaction between species i and j. For an ideal solution, the interaction between any two species is identical ($U_{ii} = U_{jj} = U_{ij}$) and the excess surface tension is zero. In this case, Eq. (86) simplifies to the ideal mixing relationship given by Eq. (26). The physical significance of the model parameters can be understood by the following: $U_{ij} - U_{ii}$ is related to the dimensionless parameter Λ_{ij} (via Eq. [87]), which accounts for the local composition effect with a normalization factor, $\sum_j x_j A_{ij}$, while $(\partial(U_{ij} - U_{ii})/\partial A)_{T,P,x}$ represents the energy change related to the increase in surface area, contributing to the excess surface tension (Li, Wang, and Wang 2000).

The above work was later extended by incorporating the NRTL equation derived by Renon (Renon and Prausnitz 1968) to represent the excess Gibbs free energy term in Eq. (83) (Li and Wang 2001). This modification results in the following equation:

$$\begin{aligned} g(T,P) &= \sum_i x_i [g_i^0(T,P) + RT\ln(x_i)] + RT \sum_i x_i \frac{\sum_j x_j G_{ji} \tau_{ji}}{\sum_l x_l G_{li}} \\ \tau_{ij} &= (U_{ij} - U_{ii})/RT \qquad\qquad G_{ji} = \exp(-\alpha_{ji}\tau_{ji}) \end{aligned} \quad . \tag{88}$$

where the non-random parameter (α) is set to 0.2, i.e., $\alpha_{ij} = \alpha_{ji} = 0.2$ (Li and Wang 2001).

Reincorporating the previous assumption that concentration and Gibbs free energy in the surface phase are proportional to those in the bulk phase yields:

$$\gamma_M = \sum_i x_i\gamma_i + RT\sum_i x_i\left[\frac{\sum_j x_j G_{ji}[1-\alpha_{ij}(\tau_{ji}-\overline{\tau_i})]}{\sum_l x_l G_{li}}\left(\frac{\partial\tau_{ji}}{\partial A}\right)_{T,P,x}\right]$$
$$\left(\frac{\partial\tau_{ji}}{\partial A}\right)_{T,P,x} = \frac{1}{RT}\left(\frac{\partial(U_{ji}-U_{ii})}{\partial A}\right)_{T,P,x} \qquad \overline{\tau_i} = \frac{\sum_l x_l G_{li}\tau_{li}}{\sum_l x_l G_{li}} \tag{89}$$

where the surface tension of pure component i is defined by $\gamma_i = (\partial g_i^{0(s)}/\partial A)_{T,P,x}$ (Li and Wang 2001). Eq. (89) is analogous to Eq. (86) in that the terms behave the same way as described previously. The difference between these equations lies in the expressions used to expand the excess molar Gibbs energy term.

5.1.10 Pandey Relation

In the 2000s, Pandey published a series of papers building on the Brock-Bird relation (Sec. 5.1.2). This work began by noting that the surface tension of a liquid mixture is not well-represented by a linear combination of the component surface tensions (Pandey and Srivastava 2010). Further, the composition at the vapor-liquid interface is different from the composition in the bulk due to migration of species with the lowest surface tension resulting in a vapor phase rich in the lowest surface tension component. The unequal nature of two-body interactions was considered by employing Flory's statistical theory for the estimation of ternary liquid system surface tension. The Corresponding States Group Contribution method was also extended to these systems.

$$\gamma = \left(\frac{\sum_i x_i P_{c_i}^*}{101.325}\right)^a \left(\sum_i x_i T_{c_i}^*\right)^b \left(c\sum_i x_i\alpha_{c_i} - d\right)\left(1-\sum_i x_i T_{r_i}^*\right)^e$$
$$\alpha_{c_i} = f\left(\frac{1+T_{br_i}^*\ln(P_{c_i}^*/101.325)}{1-T_{br_i}^*}\right) \qquad T_{r_i}^* = T/T_{c_i}^* \qquad T_{br_i}^* = T_{b_i}/T_{c_i}^* \tag{90}$$

In the above equation, T_{b_i} is the normal boiling point, $T_{c_i}^*$ is the assumed critical temperature, and $P_{c_i}^*$ is the assumed critical pressure of the i^{th} component. These critical points are calculated following group-contribution equations, given by:

$$T_{c_i}^* = \frac{T_{b_i}}{A_{T_i} + B_{T_i}\left(\sum_j n_j\Delta_{T_j}\right)_i + C_{T_i}\left(\sum_j n_j\Delta_{T_j}\right)_i^2 + D_{T_i}\left(\sum_j n_j\Delta_{T_j}\right)_i^3}$$
$$P_{c_i}^* = \frac{101.325 * \ln(T_{b_i}-273.15)}{A_{P_i} + B_{P_i}\left(\sum_j n_j\Delta_{P_j}\right)_i + C_{T_i}\left(\sum_j n_j\Delta_{P_j}\right)_i^2 + D_{P_i}\left(\sum_j n_j\Delta_{P_j}\right)_i^3} \tag{91}$$

In Eqs. (90) and (91), the terms A_T–D_T, A_P–D_P, and a–f are all constants fitted to experimental data.

5.1.11 Pockels Number Evaluation

Vakili-Nezhaad et al. performed an extensive investigation into developing an accurate predictive model for multicomponent surface tension, finding that a dimensionless group given by Eq. (92) and termed the

"Pockels Number" is a necessary aspect of translating pure component trends into a multicomponent formalism (Reza Vakili-Nezhaad et al. 2019, 2021). This Pockels Number incorporates the molar surface area (A) term described in section 5.1.6.

$$Po = \frac{\gamma A}{RT} \qquad Po_{mix} = \frac{\gamma_{mix} A}{RT} \quad . \tag{92}$$

In the above equation, R is the universal gas constant. The predictive model developed to utilize this new term is given by:

$$\gamma_{mix} = \frac{25RT}{3A}\left(1 - \left(\sum_{i=1}^{N} x_i \left(1 - \frac{3\gamma_i A}{25RT}\right)^{25/3}\right)^{3/25}\right) \qquad A = (1.02 * 10^8)\sum_{i}^{N} x_i V_i^{2/3} \quad . \tag{93}$$

Incorporating the defined Pockels Number into Eq. (93) yields:

$$Po_{mix} = \frac{25}{3}\left(1 - \left(\sum_{i=1}^{N} x_i \left(1 - \frac{3}{25} Po_i\right)^{25/3}\right)^{3/25}\right) \quad . \tag{94}$$

5.1.12 Sonawane Relation

Sonawane begins this derivation by considering a general form of the Butler equation for a binary mixture, given by:

$$\gamma_{mix} = \gamma_1 + \frac{RT}{A_1}\ln\left(\frac{x_{1,s}}{x_{1,b}}\right) \qquad \gamma_{mix} = \gamma_2 + \frac{RT}{A_2}\ln\left(\frac{x_{2,s}}{x_{2,b}}\right) \quad . \tag{95}$$

where γ_i is the pure component surface tension, A_i is the pure component molar surface area, $x_{i,s}$ refers to the component mole fraction in the surface, and $x_{i,b}$ refers to the component mole fraction in the bulk (Sonawane and Kumar 1999). Hansen and Soger presented a critical description of the equations to correlate liquid mixture surface tension using Raoult's Law (Hansen and Sogor 1972). Multiplying the equations in Eq. (95) by $x_{1,b}$ and $x_{2,b}$, respectively, and adding the resulting equations yields:

$$\gamma_{mix} = \gamma_{\text{ideal}} + RT\left(\frac{x_{1,b}}{A_1}\ln\left(\frac{x_{1,s}}{x_{1,b}}\right) + \frac{x_{2,b}}{A_2}\ln\left(\frac{x_{2,s}}{x_{2,b}}\right)\right) \qquad \gamma_{\text{ideal}} = \gamma_1 x_{1,b} + \gamma_2 x_{2,b} \quad . \tag{96}$$

Estimating mixture surface tension via Eq. (96) requires knowledge of both the bulk and surface mole fractions. The relationship between bulk and surface mole fractions can be estimated under certain conditions by considering a dimensionless difference parameter (δ), comprising two components, δ_p and δ_m.

$$\begin{aligned} x_{1,s} &= x_{1,b} + x_{1,b}x_{2,b}\delta_p + x_{1,b}X_{2,b}^2\delta_m \\ x_{2,s} &= x_{2,b} + x_{1,b}x_{2,b}\delta_p - x_{1,b}X_{2,b}^2\delta_m \end{aligned} \quad . \tag{97}$$

Manipulating Eq. (97) allows a derivation of the ratios of mole fractions in the bulk and surface phases, given by:

$$\begin{aligned} \ln\left(\frac{x_{1,s}}{x_{1,b}}\right) &= \ln\left(1 + x_{2,b}\delta_p + x_{2,b}^2\delta_m\right) = \ln\left(1 + x_{2,b}\delta\right) \\ \ln\left(\frac{x_{2,s}}{x_{2,b}}\right) &= \ln\left(1 + x_{1,b}\delta_p - x_{1,b}x_{2,b}\delta_m\right) = \ln\left(1 + x_{1,b}\delta\right) \\ \delta &= \delta_p + \delta_m x_{2,b} \end{aligned} \quad . \tag{98}$$

Substituting the above equation into Eq. (96) yields:

$$\gamma_{mix} = \gamma_{\text{ideal}} + RT\left(\frac{x_{1,b}}{A_1}\ln\left(1 + x_{2,b}\gamma_{mix}\right) + \frac{x_{2,b}}{A_2}\ln\left(1 - x_{1,b}\gamma_{mix}\right)\right) \quad . \tag{99}$$

Because the product of mole fractions with δ is << 1, expansion of the logarithmic terms to their first term yields:

$$\gamma_{mix} = \gamma_{\text{ideal}} + RTx_1x_2\left(\frac{1}{A_1} - \frac{1}{A_2}\right)\delta \quad , \tag{100}$$

where binary mixtures yield $x_{1,b} = x_1$ and $x_{2,b} = x_2$, leading to:

$$\gamma_{mix} = \gamma_{\text{ideal}} + RTx_1x_2\left(\frac{1}{A_1} - \frac{1}{A_2}\right)\left(\delta_p + \delta_m x_2\right) \quad . \tag{101}$$

Thus, Eq. (101) is a complete working equation for binary mixture surface tension with the two unknown parameters, δ_p and δ_m, determined by fitting experimental data for surface tension vs. composition (Sonawane and Kumar 1999).

5.2 PRELIMINARY USE OF LARGE LANGUAGE MODELS FOR DATA COLLECTION OF MS THERMOPHYSICAL PROPERTIES

A preliminary exploration of large language models (LLMs) was conducted to assist in data mining for molten salt properties reported in the literature. The approach used herein contrasts with the typically employed method of manually searching the literature based on keywords for data. Given the future need to incorporate data derived from either MD simulations or experiments, it will be advantageous to employ LLMs for the sake of reducing the time burden associated with the data collection process across the entire compositional range of MSTDB-TP. Obviously, there will be an ongoing need to evaluate individual data sources to ensure that high-quality data are being incorporated into MSTDB-TP. The preliminary effort described herein did not necessarily focus on MD data, but future implementations can be more targeted toward that category of references.

In this initial trial, the focus was on evaluating and comparing the ability of several LLMs to identify reported values of density, viscosity, thermal conductivity, and heat capacity for specific mixtures: UCl_3 or UCl_4 with $AlCl_3$ or $MgCl_2$, and UF_4 with KF, BeF_2, or ThF_4. The comparison included four widely accessible LLMs: ChatGPT (OpenAI), Gemini (Google), Claude (Anthropic), and Platform (FutureHouse). The Platform LLM offers three distinct modes: Crow, optimized for concise answers with citations; Falcon, designed for in-depth searches of publications and reports; and Owl, tailored for quick retrieval of prior work. These models were tested with different prompt strategies to retrieve relevant property data for the target molten salt mixtures. Many queries returned "no results," reflecting the general scarcity of published experimental data. Among the tested systems, the Falcon mode of Platform demonstrated the strongest performance, often locating density data and, to a lesser extent, values for other properties, supported by references to original reports, theses, or publications. In contrast, general-purpose LLMs (e.g., ChatGPT) often generated fabricated references to non-existent publications. Moving forward, our prompting strategies will be refined to broaden the scope of searches and enhance the reliability of retrievable information.

Table 5. Correlations found in literature for multicomponent system surface tension

Correlation	Required Input Data
Ideal Mixing	Component mole fraction (x_i), component surface tension (γ_i)
Non-ideal Binary Mixing	Component mole fraction (x_i), component surface tension (γ_i), binary interaction parameter (C_i)
Brock-Bird	Component mole fraction (x_i), component boiling temperature (T_{bi}), component critical temperature (T_{ci}), component critical pressure (P_{ci})
Butler	Component bulk mole fraction (x_i), component surface mole fraction (x_i^s), pure component surface tension (γ_i^*), bulk activity coefficient (α), surface activity coefficient (α^s), pure component molar surface area (A_i^*), partial molar surface area ($\overline{A}$)
Dutcher	Component mole fraction (x_i), pure component surface tension (γ_i), binary interaction parameters ($a_{ij},\ b_{ij}(T)$)
Eberhart (Binary)	Component mole fraction (x_i), pure component surface tension (γ_i), binary interaction parameter (S_{12})
Eberhart (Multicomponent)	Component mole fraction (x_i), pure component surface tension (γ_i), binary interaction parameter ($S_{ij},\ i \neq j$)
Goldsack & Sarvas	Component mole fraction (x_i), component molar volume (V_i)
Hu	Component mole fraction in surface (x_{iS}) and bulk (x_{iB}) phases, component molar volume (V_i), pure component surface tension (γ_i), pressure in surface (P_S) and bulk (P_B) phases, van der Waals equation parameters (a_i and b_i) for each component
Kleinheins	Component mole fraction (x_i), pure component surface tension (γ_i), separation factors (S_{ij}) for each pairwise combination of components, bulk (B_{ij}) and surface (A_{ij}) non-ideality factors for each pairwise combination of components
Li	Component mole fraction (x_i), pure component surface tension (γ_i), molar Gibbs free energy (g_i^0), component molar volume (v_i), molecular pair interaction energy (U_{ii}, U_{ij}), fitted non-random two-liquid parameter (α)
Pandey[1]	Component mole fraction (x_i), component boiling temperature (T_{b_i}), component critical temperature ($T_{c_i}^*$), component critical pressure ($P_{c_i}^*$)
Pockels Number	Component mole fraction (x_i), pure component surface tension (γ_i), component molar volume (V_i)
Sonawane	Component mole fraction (x_i), pure component surface tension (γ_i), fitting parameters (δ_p, δ_s)

[1] Includes group contribution methodology to determine critical temperature and critical pressure based on boiling temperature and fitted experimental parameters.

Table 6. References found by preliminary use of LLMs to fill gaps within MSTDB-TP

	Density	Viscosity	Thermal Conductivity	Heat Capacity
UCl_3-$AlCl_3$	Not found	Not found	Not found	Not found
UCl_3-$MgCl_2$	(Li, Dai, and Jiang 2022)	(Jung et al. 2023)	Not found	Not found
UCl_4-$AlCl_3$	Not found	Not found	Not found	Not found
UCl_4-$MgCl_2$	(Katyshev and Desyatnik 1981)	Not found	Not found	Not found
UF_4-KF	(Karlsson et al. 2023)	(Jerden 2019)	(Beneš and Konings 2009)	(Cohen, Powers, and Greene 1956)
UF_4-BeF_2	(Cohen, Powers, and Greene 1956)	Not found	(Beneš and Konings 2009)	(Park 2024)
UF_4-ThF_4	(Wang and Maschek 2010)	(Beneš and Konings 2009)	(Mastromarino 2022)	Not found

6. ACCESS INSTRUCTIONS

The databases and associated documents are hosted on a publicly accessible, permission-protected server at ORNL: https://code.ornl.gov/neams/mstdb/. Access requires an account on the ORNL/ITSD GitLab server and an MSTDB membership, which, once granted, allows users to download all files.

ORNL is participating in OneID, an identity federation managed by DOE. ORNL employees can use the ORNL AzureAD login button for single sign-on, or the ORNL Yubikey login button to sign in with a certificate.

External collaborators can use the OneID login button to log in using an HSPD-12 PIV badge, a common access card (CAC), or credentials for one of the participating labs shown on the OneID screen. If you do not have a qualified badge or do not see your organization among the OneID choices, click the icon for Login.Gov and create an account. If you use the same email address for login.gov that you have registered in the past with XCAMS, your account will automatically be linked.

If you are logging into the GitLab server for the first time, be sure to take note of your username (e.g., @JohnDoe).

To Request MSTDB membership, please fill out the form at https://mstdb.ornl.gov/mstdb-signup/ with all necessary information. Doing so will notify the MSTDB team, and you will be added to the database on the closest Tuesday or Thursday relative to submission of the form.

If you are not automatically added to the GitLab project for MSTDB by the end of the closest Tuesday or Thursday relative to submission of the form, email mstdb@ornl.gov to inform that you have submitted the MSTDB sign-up form and you are awaiting access to the project.

7. CONCLUSION

The Molten Salt Thermal Properties Database – Thermophysical (MSTDB-TP) underwent continued development to support an update from version 3.1 to version 4.0. The most significant update is the incorporation of surface tension data. Version 4.0 incorporates surface tension correlations for 294 unique chloride and fluoride salt compositions, including 29 pure components, 108 pseudobinary systems, 91 pseudoternary systems, and 66 pseudoquaternary systems. These correlations were selected based on a quality assessment methodology for comparing and ranking the level of detail provided with published experimental data sets. This addition has expanded the database to 976 unique salt compositions for which thermophysical property data have been evaluated. This continued expansion reinforces the capabilities of MSTDB-TP to support thermal hydraulic and multiphysics simulation of MSRs using the most accurate data available. The impact of this effort is evidenced by the continual growth in number and distribution of users, reaching over 400 subscribers across the world including national labs, universities, government, and industry. This version update also included the implementation of JSON file architecture. This format allows the integration of thermophysical property data, compositions, reference information (citation and DOI), and RK parameters for density and viscosity. Previously, this information was spread across four CSV files, which remain available for users who might prefer the format.

Predictive capabilities were also expanded in version 4.0. The RK implementation in Saline allows estimation capabilities beyond the ideal mixing model, improving the expected accuracy of the estimation. An additional alteration of Saline data implementation involves applying RK estimation smoothly across the compositional space of molten salt mixtures, as opposed to the previously discontinuous application in which exact compositional matches refer to experimental data. Future work is planned to incorporate a tuning parameter that allows the user to decide when direct experimental results are used. The RK estimation capability was also integrated into the GUI, in addition to ideal mixing extrapolation, to allow density and viscosity prediction based on available data and produce composition-dependent figures of results. However, due to a lack of experimental data, RK expansion does not produce dependable estimates for thermal conductivity. Thus, a kinetic theory approach adapted from the literature was modified to be more generalizable to molten salts including actinides, involving estimated or modeled endmember parameters with no compositional data required. This enhanced technique was further validated using salt system data already in MSTDB-TP.

Plans for future iterations of MSTDB-TP include expanding the database to incorporate the latest experimental studies of thermophysical properties, testing predictive models for multicomponent surface tension, developing more rapid methods for MD and experimental data collection, and adopting a quality ranking methodology for assessment of molecular dynamics studies. Several potential multicomponent surface tension models were preliminarily identified involving a wide range of input parameters from thermodynamic properties to material interactions. Based on recently incorporated correlations for several multicomponent systems across a wide compositional space, these models will be evaluated for accuracy, applicability, and further development. Preliminary work was conducted to incorporate LLMs to aid in the identification of MD and experimental reference data for molten salt thermophysical properties. Several models and search modes were tested with different prompt strategies, resulting in a range of outcomes from hallucinating non-existent references to limited success reflecting the scarcity of published data. Future work involves refining the prompt strategy to broaden the search scope and enhance the reliability of retrieved information. Finally, as MD simulations for molten salt property determination continue to develop, a strategy must be established to compare the quality of published literature in a manner similar to that shown in Table 2 for experimental data. This may involve, for example, replacing the environmental control aspect with simulation system size and replacing the measurement precision aspect with simulation duration.

8. REFERENCES

Abeles, B. 1963. "Lattice thermal conductivity of disordered semiconductor alloys at high temperatures." *Physical Review* 131 (5): 1906.

Agca, C., and J. W. McMurray. 2022. "Empirical estimation of densities in NaCl-KCl-UCl_3 and NaCl-KCl-YCl_3 molten salts using Redlich-Kister expansion." *Chemical Engineering Science* 247 (January): 117086. ISSN: 0009-2509. https://doi.org/10.1016/J.CES.2021.117086.

Andersson, DA, and Ben W Beeler. 2022. "Ab initio molecular dynamics (AIMD) simulations of NaCl, UCl3 and NaCl-UCl3 molten salts." *Journal of Nuclear Materials* 568:153836.

Ard, Johnathon C, Juliano Schorne-Pinto, Mina Aziziha, Jacob A Yingling, Amir M Mofrad, Tristan J Johnson, Clara M Dixon, and Theodore M Besmann. 2023. "Thermodynamic assessments or re-assessments of 30 pseudo-binary and-ternary salt systems." *The Journal of Chemical Thermodynamics* 177:106931.

Ard, Johnathon C, Jacob A Yingling, Tristan J Johnson, Juliano Schorne-Pinto, Mina Aziziha, Clara M Dixon, Matthew S Christian, Jacob W McMurray, and Theodore M Besmann. 2022. "Development of the molten salt thermal properties database- thermochemical (MSTDB- TC), example applications, and LiCl- RbCl and UF3- UF4 system assessments." *Journal of Nuclear Materials* 563:153631.

Barthle, Jonathan L, Bailey Bertrand, Edward M Duchnowski, Brian D Wirth, and Nicholas R Brown. 2024. "Sensitivity analysis and fuel performance of a control rod withdrawal in the generic fluoride-salt-cooled high temperature reactor." *Nuclear Engineering and Design* 428:113529.

Beneš, O, and RJM Konings. 2009. "Thermodynamic properties and phase diagrams of fluoride salts for nuclear applications." *Journal of Fluorine Chemistry* 130 (1): 22–29.

Besmann, Theodore M, and Juliano Schorne-Pinto. 2021. "Developing practical models of complex salts for molten salt reactors." *Thermo* 1 (2): 168–178.

Besmann, Theodore M, Juliano Schorne-Pinto, Mina Aziziha, Amir M Mofrad, Ronald E Booth, Jacob A Yingling, Jorge Paz Soldan Palma, Clara M Dixon, Jack A Wilson, and Donny Hartanto. 2024. "Applications of Thermochemical Modeling in Molten Salt Reactors." *Materials* 17 (2): 495.

Birri, A., R. Gallagher, C. Agca, J. McMurray, and N. D. Ezell. 2022. "Application of the Redlich-Kister expansion for estimating the density of molten fluoride psuedo-ternary salt systems of nuclear industry interest." *Chemical Engineering Science* 260 (October): 117954. ISSN: 0009-2509. https://doi.org/10.1016/J.CES.2022.117954.

Birri, Anthony, Nick Termini, Kevin Garland, Shay Chapel, Hunter Andrews, Paul Rose Jr., and N. Dianne Bull Ezell. 2023. *FY23 Progress Report on Viscosity and Thermal Conductivity Measurements of Molten Salts.* Technical report. ORNL/TM-2023/3048. Oak Ridge National Lab.(ORNL), Oak Ridge, TN (United States).

Birri, Tony, Nick Termini, Ryan Chesser, Shane Henderson, Jacob Numbers, Ethan Wilgocki, and N. Dianne Bull Ezell. 2024. *An Overview of the Molten Salt Thermal Properties Database–Thermophysical, Version 3.1 (MSTDB-TP v.3.1).* Technical report. Oak Ridge National Laboratory (ORNL), Oak Ridge, TN (United States).

Blanke, BC, EN Bousquet, LV Jones, EL Murphy, and RE Vallee. 1958. *Density of fused mixtures of sodium fluoride, beryllium fluoride, and uranium fluoride.* Technical report. Mound Plant (MOUND), Miamisburg, OH (United States).

Blanke, BC, KW Foster, LV Jones, KC Jordan, RW Joyner, and EL Murphy. 1958. *Viscosity of fused mixtures of sodium fluoride, beryllium fluoride, and uranium fluoride.* Technical report. Mound Plant (MOUND), Miamisburg, OH (United States).

Bobrova, KO, VN Dokutovich, and PN Mushnikov. 2023. "Thermophysical properties of several molten mixtures of the LiF–BeF2–UF4 system." *Russian Metallurgy (Metally)* 2023 (2): 126–135.

Bray, Tim. 2017. *The JavaScript Object Notation (JSON) Data Interchange Format.* RFC 8259, 8259, December. https://doi.org/10.17487/RFC8259. https://www.rfc-editor.org/info/rfc8259.

Brock, J.R., and R.B. Bird. 1955. "Surface Tension and the Principle of Corresponding States." *AIChE Journal* 1 (2): 174–177.

Butler, J.A.V. 1932. "The Thermodynamics of the Surfaces of Solutions." *Proceedings of the Royal Society of London, Series A* 135 (827): 348–375.

Cantor, S. 1973. *Density and viscosity of several molten fluoride mixtures.* Technical report. Oak Ridge National Lab., Tenn. (USA), February. https://doi.org/10.2172/4419855. https://www.osti.gov/biblio/4419855.

Cantor, S., W. T. Ward, and C. T. Moynihan. 1969. "Viscosity and Density in Molten BeF2–LiF Solutions." *The Journal of Chemical Physics* 50, no. 7 (April): 2874–2879. ISSN: 0021-9606. https://doi.org/10.1063/1.1671478. eprint: https://pubs.aip.org/aip/jcp/article-pdf/50/7/2874/18861111/2874_1_online.pdf. https://doi.org/10.1063/1.1671478.

Chunxi, L., W. Wenchuan, and W. Zihao. 2000. "A Surface Tension MOdel for Liquid Mixtures Based on the Wilson Equation." *Fluid Phase Equilibria* 175:185–196. https://doi.org/https://doi-org.ornl.idm.oclc.org/10.1016/S0378-3812(00)00447-7.

Cohen, SI, WD Powers, and ND Greene. 1956. *A physical property summary for ANP fluoride mixtures.* Technical report. Oak Ridge National Laboratory (ORNL), Oak Ridge, TN (United States).

Conway, B.E. 1976. "Hydrophobic and Electrostatic Interactions in Adsorption at Interfaces: Relation to the Nature of Liquid Surfaces." *Croatica Chemica Acta* 48 (4): 573–596.

Cooke, JW, HW Hoffman, and JJ Keyes Jr. 1969. "Semiannual progress report for period ending February 28, 1969." Chap. Heat Transfer and thermophysica properties. Oak Ridge National Laboratory.

Crawford, S, and S Lee. 2024. "Comprehensive Simulation of the Integral Molten Salt Reactor (IMSR) Using a Lumped 3D Modeling Approach." *Proceedings of the Canadian Nuclear Society.*

Dolan, Thomas James. 2017. *Molten salt reactors and thorium energy.* Woodhead Publishing.

Duemmler, Kai, David Andersson, and Benjamin Beeler. 2024. "First-principles investigation of the thermophysical properties of NaCl, PuCl3, and NaCl-PuCl3 Molten salts." *Journal of Nuclear Materials* 591:154902. ISSN: 0022-3115. https://doi.org/https://doi.org/10.1016/j.jnucmat.2024.154902. https://www.sciencedirect.com/science/article/pii/S0022311524000072.

Dutcher, C.S., A.S. Wexler, and S.L. Clegg. 2010. "Surface Tensions of Inorganic Multicomponent Aqueous Electrolyte Solutions and Melts." *Journal of Physical Chemistry A* 114:12216–12230.

Eberhart, J.G. 1966. "The Surface Tension of Binary Liquid Mixtures." *The Journal of Physical Chemistry* 70 (4): 1183–1186.

El Haber, M., C. Ferronato, A. Giroir-Fendler, L. Fine, and B. Nozière. 2023. "Salting Out, Non-Ideality and Synergism Enhance Surfactant Efficiency in Atmospheric Aerosols." *Scientific Reports* 13 (20672). https://doi.org/https://doi.org/10.1038/s41598-023-48040-5.

Fainerman, V.B., R. Miller, and E.V. Aksenenko. 2002. "Simple Model for Prediction of Surface Tension of Mixed Surfactant Solutions." *Advances in Colloid and Interface Science* 96 (1–3): 339–359. https://doi.org/https://doi-org.ornl.idm.oclc.org/10.1016/S0001-8686(01)00088-4.

Gallagher, Ryan C, Anthony Birri, Nick G Russell, Anh-Thu Phan, and Aïmen E Gheribi. 2022. "Investigation of the thermal conductivity of molten LiF-NaF-KF with experiments, theory, and equilibrium molecular dynamics." *Journal of Molecular Liquids* 361:119151.

Gardner, LD, KA Chamberlain, and MA Rose. 2024. *Property Measurements of LiF-NaF-KF Molten Salts Doped with Surrogate Fission Products.* Technical report. Argonne National Laboratory (ANL), Argonne, IL (United States).

Gheribi, Aïmen E, and Patrice Chartrand. 2016. "Thermal conductivity of molten salt mixtures: Theoretical model supported by equilibrium molecular dynamics simulations." *The Journal of chemical physics* 144 (8).

Gheribi, Aïmen E, Anh Thu Phan, and Patrice Chartrand. 2022. "A theoretical framework for reliable predictions of thermal conductivity of multicomponent molten salt mixtures: KCl-NaCl-MgCl2 as a case study." *Solar Energy Materials and Solar Cells* 236:111478.

Gheribi, Aïmen E, Anh Thu Phan, Huiqiang Yang, Ryan C Gallagher, and Patrice Chartrand. 2024. "The role of the local structure on the thermal transport within dissociated and complexed molten salt mixtures." *Journal of Molecular Liquids,* 125239.

Gheribi, Aïmen E, Sándor Poncsák, Rémi St-Pierre, László I Kiss, and Patrice Chartrand. 2014. "Thermal conductivity of halide solid solutions: Measurement and prediction." *The Journal of Chemical Physics* 141 (10).

Gheribi, Aïmen E, Mathieu Salanne, and Patrice Chartrand. 2016. "Formulation of temperature-dependent thermal conductivity of NaF, β-Na3AlF6, Na5Al3F14, and molten Na3AlF6 supported by equilibrium molecular dynamics and density functional theory." *The Journal of Physical Chemistry C* 120 (40): 22873–22886.

Gheribi, Aïmen E, Jesus A Torres, and Patrice Chartrand. 2014. "Recommended values for the thermal conductivity of molten salts between the melting and boiling points." *Solar energy materials and solar cells* 126:11–25.

Goldsack, D.E., and C.D. Sarvas. 1981. "Volumte Fraction Statistics and the Surface Tension of Non-electrolyte Solutions." *Canadian Journal of Chemistry* 59 (20): 2968–2980.

Hansen, R.S., and L. Sogor. 1972. "Surface Tension of Binary Solutions of Non-Electrolytes." *Journal of Colloid and Interface Science* 40 (3): 424–428. https://doi.org/https://doi-org.ornl.idm.oclc.org/10.1016/0021-9797(72)90352-9.

Henderson, S., C. Agca, J. W. McMurray, and R. A. Lefebvre. 2021. *Saline: An API for Thermophysical Properties.* Technical report. Oak Ridge National Laboratory (ORNL), Oak Ridge, TN (United States).

Hu, Y. 1983. *Molecular Thermodynamics of Fluid (in Chinese).* Higher Educational Publisher, Beijing.

Hu, Y., Z. Li, J. Lu, Y. Li, and Y. Jin. 1997. "A New Model for the Surface Tension of Binary and Ternary Liquid Mixtures Based on Peng-Robinson Equation of State." *Chinese Journal of Chemical Engineering* 5 (3): 193–199.

Hua, X.Y., and M.J. Rosen. 1982. "Synergism in Binary Mixtures of Surfactants: I. Theoretical Analysis." *Journal of Colloid and Interface Science* 90 (1): 212–219. https://doi.org/https://doi-org.ornl.idm.oclc.org/10.1016/0021-9797(82)90414-3.

Jerden, James. 2019. *Molten salt thermophysical properties database development: 2019 update.* Technical report. Argonne National Lab.(ANL), Argonne, IL (United States).

Jiang, Chao, Jicheng Guo, David Andersson, Daniel Schwen, Chris Benmore, Nathaniel Hoyt, and Benjamin Spencer. 2024. "Predicting thermophysical properties of molten salts in the MgCl2-NaCl-KCl-LiCl system with a shell-model potential." *Journal of Molecular Liquids* 403:124854.

Jung, Chan-Yong, Eunkyeom Lee, Tae-Hyeong Kim, and Jong-Yun Kim. 2023. "Viscosity of Molten Salt Systems: NaCl-MgCl2 and NaCl-MgCl2-UCl3." *Proceedings of the Korean Radioactive Waste Society (in Korean)* 21 (1): 474–474.

Karlsson, Toni Y, Scott C Middlemas, Manh-Thuong Nguyen, Michael E Woods, Kevin R Tolman, Vassiliki-Alexandra Glezakou, Steven D Herrmann, Juliano Schorne-Pinto, Ryan D Johnson, Shawn E Reddish, et al. 2023. "Synthesis and Thermophysical Property Determination of NaCl-PuCl3 Salts." *Journal of Molecular Liquids,* 122636.

Kato, Yoshio, Kazuo Furukawa, Nobuyuki Araki, and Kiyosi Kobayasi. 1983. "Thermal diffusivity measurement of molten salts by use of a simple ceramic cell." *High Temp.-High Pressures;(United Kingdom)* 15 (2).

Katyshev, Sergey Filippovich. 2001. "Svoystva rasplavov smesey galogenidov shchelochnykh metallov, tsirkoniy, gafniy i uran." PhD diss., Ural State Technical University.

Katyshev, SF, and VN Desyatnik. 1981. "Density and surface tension of uranium tetrachloride melts with magnesium and calcium chlorides." *Soviet Atomic Energy* 51 (6): 810–812.

Khokhlov, V, I Korzun, V Dokutovich, and E Filatov. 2011. "Heat capacity and thermal conductivity of molten ternary lithium, sodium, potassium, and zirconium fluorides mixtures." *Journal of nuclear materials* 410 (1-3): 32–38.

Kleinheins, J., C. Marcoli, C.S. Dutcher, and N. Shardt. 2024. "A Unified Surface Tension Model for Multi-component Salt, Organic, and Surfactant Solutions." *Physical Chemistry Chemical Physics* 26:17521–17538.

Kleinheins, J., N. Shardt, M.E. Haber, C. Ferronato, B. Nozière, T. Peter, and C. Marcolli. 2023. "Surface Tension Models for Binary Aqueous Solutions: A Review and Intercomparison." *Physical Chemistry Chemical Physics* 25 (16): 11055–11074.

Klemens, PG. 1955. "The scattering of low-frequency lattice waves by static imperfections." *Proceedings of the Physical Society. Section A* 68 (12): 1113.

Krepel, Jiri, and Kevin J Kramer. 2024. "TerraPower fast chloride reactor." In *Molten Salt Reactors and Thorium Energy,* 953–972. Elsevier.

Li, Bo, Sheng Dai, and De-en Jiang. 2022. “First-principles molecular dynamics simulations of UCl n–MgCl 2 (n= 3, 4) molten salts.” *Physical Chemistry Chemical Physics* 24 (39): 24281–24289.

Li, C., and W. Wang. 2001. “A Surface Tension Model for Liquid Mixtures Based on NTRL Equation.” *Chinese Journal of Chemical Engineering* 9 (1): 45–50.

Li, C., W. Wang, and Z. Wang. 2000. “A Surface Tension Model for Liquid Mixtures Based on the Wilson Equation.” *Fluid Phase Equilibria* 175:185–196.

Lonergan, Jason, Vitaliy Goncharov, Michaella Swinhart, Kyle Makovsky, Mark Rollog, Bruce McNamara, Richard Clark, Derek Cutforth, Christopher Armstrong, Xiaofeng Guo, et al. 2023. “Thermodynamic investigation of the NaCl-KCl salt system from 25 to 950° C.” *Journal of Molecular Liquids* 391:122591.

Makovsky, Kyle, Michaella Harris, Ji-Hye Seo, Kent Detrick, Jose Marcial, Dallin Barton, and Jacqueline Roye. 2024. *Experimental Investigation into Select Thermophysical Properties of the Potassium-Magnesium Chloride Salt System for Molten Salt Reactors.* Technical report. PNNL-37190. Pacific Northwest National Laboratory.

Mastromarino, S. 2022. *New measurement methods and physico-chemical properties of the MSFR salt.* Technical report.

Mcmurray, Jake W, Kaitlin Johnson, Can Agca, Benjamin R Betzler, Dave J Kropaczek, Theodore M Besmann, David Andersson, and N Ezell. 2021. *Roadmap for thermal property measurements of Molten Salt Reactor systems.* Technical report. Oak Ridge National Laboratory (ORNL), Oak Ridge, TN (United States).

Merritt, Brian, Michael Seneca, Ben Wright, Noah Cahill, Noah Petersen, Austin Fleming, and Troy Munro. 2022. “Thermal conductivity characterization of fluoride and chloride molten salts using a modified transient hot-wire needle probe.” *International Journal of Thermophysics* 43 (10): 149.

Nguyen, Manh-Thuong, Michael E Woods, Juliano Schorne-Pinto, Nick H Erfurth, Scott C Middlemas, and Toni Karlsson. 2025. “Thermophysical Properties of NaCl–UCl3–PuCl3 Molten Salts: A Combined Computational and Experimental Study.” *ACS Applied Energy Materials* 8 (10): 6482–6491.

Pandey, J.D., and T. Srivastava. 2010. “Surface Tension — A Theoretical Study of Multicomponent Solutions.” *Journal of Molecular Liquids* 155:51–56.

Park, Jaewoo. 2024. *Studies on Molten Salt Fuels: Properties, Purification, and Materials Degradation.* Technical report. Virginia Tech.

Parker, Stephen Scott, A Long, C Lhermitte, S Vogel, M Monreal, and JM Jackson. 2022. “Thermophysical properties of liquid chlorides from 600 to 1600 K: Melt point, enthalpy of fusion, and volumetric expansion.” *Journal of Molecular Liquids* 346:118147.

Peng, D.Y., and D.B. Robinson. 1976. “New Two-Constant Equation of State.” *Industrial & Engineering Chemistry Fundamentals* 15 (1): 59–64. https://doi.org/http://dx.doi.org/10.1021/i160057a011.

Qiao, Zhiya, Lijun Yan, Zhanmin Cao, and Yunan Xie. 2001. “Surface tension prediction of high-temperature melts.” *Journal of Alloys and Compounds* 325 (1): 180–189. ISSN: 0925-8388. https://doi.org/https://doi.org/10.1016/S0925-8388(01)01362-7. https://www.sciencedirect.com/science/article/pii/S0925838801013627.

Redkin, Alexander, Evgeniya Il'ina, Svetalana Pershina, Peter Mushnikov, Sergey Stankus, Alibek Agazhanov, Yuriy Zaikov, Anna Kholkina, and Artyem Artamonov. 2022. "Thermal Properties of Li2BeF4 near Melting Point." *Thermo* 2 (3): 107–115.

Renon, H., and J.M. Prausnitz. 1968. "Local Compositions in Thermodynamic Excess Functions for Liquid Mixtures." *AIChE Journal* 14 (1): 135–144. https://doi.org/https://doi.org/10.1002/aic.690140124.

Reza Vakili-Nezhaad, G., M. Al-Wadhahi, S. Al-Haddabi, A. Vakilinejad, and W.E. Acree. 2019. "Surface Tension of Multicomponent Organic Mixtures: Measurement and Correlation." *Journal of Molecular Liquids* 296:112008.

———. 2021. "Surface Tension of Binary Organic Mixtures Based on a New Dimensionless Number." *Journal of Chemical Thermodynamics* 152:106292.

Roper, Robin, Megan Harkema, Piyush Sabharwall, Catherine Riddle, Brandon Chisholm, Brandon Day, and Paul Marotta. 2022. "Molten salt for advanced energy applications: A review." *Annals of Nuclear Energy* 169:108924.

Rose, MA, LD Gardner, TT Lichtenstein, SA Thomas, and E Wu. 2023. *Property Measurements of NaCl-UCl3 and NaCl-KCl-UCl3 Molten Salts.* Technical report. ANL/CFCT-22/45 Rev. 1. Argonne National Laboratory (ANL), Argonne, IL (United States).

Rose, Melissa A. 2022. *Quality Ranking System for Molten Salt Thermal Property Data.* Technical report. ANL/CFCT-22/26. Argonne National Laboratory (ANL), Argonne, IL (United States).

———. 2023. *Quality Ranking of Unary Fluoride Salt Property Data in MSTDB-TP.* Technical report. ANL/CFCT-23/48. Argonne National Laboratory (ANL), Argonne, IL (United States).

Ross, R G, P Andersson, B Sundqvist, and G Backstrom. 1984. "Thermal conductivity of solids and liquids under pressure." *Reports on Progress in Physics* 47:1347.

Rudenko, A, A Redkin, P Mushnikov, E Il'ína, S Pershina, O Tkacheva, Yu Zaikov, and S Kumkov. 2024. "Thermal Properties of Some Molten Mixtures in System (NaF-KF) eut–UF4." *International Journal of Thermophysics* 45 (8): 114.

Rudenko, AV, AA Redkin, AY Galashev, KA Abramova, OR Rakhmanova, EA Il'ina, SV Pershina, and Yu P Zaikov. 2024. "Thermal Properties of NaF–KF and NaF–KF–MgF2 Molten eutectic Mixtures: Experiment and Simulation." *International Journal of Thermophysics* 45 (4): 47.

Salko Jr, Robert, Travis Mui, Rui Hu, and Elia Merzari. 2021. *Implementation of a Drift-Flux Model in SAM for Modeling of Passively Transported Gas in Molten Salt Reactors.* Technical report. Oak Ridge National Laboratory (ORNL), Oak Ridge, TN (United States).

Shardt, N., and J.A.W. Elliott. 2017. "Model for the Surface Tension of Dilute and Concentrated Binary Aqueous Mixtures as a Function of Composition and Temperature." *Langmuir* 33 (41): 11077–11085.

Smith, Nicholas Vise, William C Phillips, James A King, Jacob Allen Yingling, Jonathon Powell Wilcox, Michael Ellis Woods, and Toni Y Karlsson. 2024. *Natura Resources Molten Salt Research Reactor (MSRR) Fuel Workshop: Summary Report.* Technical report. Idaho National Laboratory (INL), Idaho Falls, ID (United States).

Soledade C. S. Santos, M., and J.C.R. Reis. 2021. "Examination of the Butler Equation for the surface Tension of Liquid Mixtures." *ACS Omega* 6 (33): 21571–21578.

Sonawane, P.D., and A. Kumar. 1999. “A New Equation for the Correlation of Surface Tension-Composition Data of Solvent-Solvent and Solvent-Fused Salt Mixtures.” *Fluid Phase Equilibria* 157:17–28.

Sorensen, Kirk. 2016. “Liquid-fluoride thorium reactor development strategy.” In *Thorium Energy for the World: Proceedings of the ThEC13 Conference, CERN, Globe of Science and Innovation, Geneva, Switzerland, October 27-31, 2013,* 117–121. Springer.

Spencer, Benjamin W, and Theodore M Besmann. 2022. *Integration Plan for NEAMS Structural Materials and Chemistry MSR Modeling.* Technical report. Idaho National Laboratory (INL), Idaho Falls, ID (United States).

Strzelecki, Andrew C, S Scott Parker, Shane C Mann, David C Arellano, Sarah M Hickam, S Douglas Ware, Nathan A Conroy, Hakim Boukhalfa, Titus YP De Jong, David A Andersson, et al. 2025. “Determination of thermochemical properties of the molten PuCl3-NaCl eutectic mixture by high-temperature drop calorimetry.” *Journal of Molecular Liquids* 424:127073.

Termini, Nick, Anthony Birri, Shane Henderson, and N. Dianne Bull Ezell. 2023. *An Overview of the Molten Salt Thermal Properties Database–Thermophysical, Version 2.1.1 (MSTDB-TP v.2.1.1).* Technical report. Oak Ridge National Laboratory (ORNL), Oak Ridge, TN (United States).

Termini, Nick, Tony Birri, Brett Smith, Ryan Chesser, Jacob Numbers, Kevin Garland, Ethan Wilgocki, Craig Gray, and Vanda Glezakou. 2024. *FY24 Progress Report on Viscosity and Thermal Conductivity Measurements of Nuclear Industry Relevant Chloride Salts: An Experimental and Computational Study.* Technical report. Oak Ridge National Laboratory (ORNL), Oak Ridge, TN (United States).

Triplett, K.A., S.M. Ghiaasiaan, S.I. Abdel-Khalik, A. LeMouel, and B.N. McCord. 1999. “Gas–liquid two-phase flow in microchannels: Part II: void fraction and pressure drop.” *International Journal of Multiphase Flow* 25 (3): 395–410. ISSN: 0301-9322. https://doi.org/https://doi.org/10.1016/S0301-9322(98)00055-X. https://www.sciencedirect.com/science/article/pii/S030193229800055X.

Walz, Marie-Madeleine, and David Van der Spoel. 2021. “Microscopic origins of conductivity in molten salts unraveled by computer simulations.” *Communications Chemistry* 4 (1): 9.

Wang, Shisheng, and Werner Maschek. 2010. “A Statistical Mechanical Equation of State for Fluid UF4 and ThF4.” In *International Conference on Nuclear Engineering,* 49323:323–331.

Wang, Xiaoxin, Jesus Del Rincon, Peiwen Li, Youyang Zhao, and Judith Vidal. 2021. “Thermophysical properties experimentally tested for NaCl-KCl-MgCl2 eutectic molten salt as a next-generation high-temperature heat transfer fluids in concentrated solar power systems.” *Journal of Solar Energy Engineering* 143 (4): 041005.

Xu, Xiankun, Xiaoxin Wang, Peiwen Li, Yuanyuan Li, Qing Hao, Bo Xiao, Hassan Elsentriecy, and Dominic Gervasio. 2018. “Experimental test of properties of KCl–MgCl2 eutectic molten salt for heat transfer and thermal storage fluid in concentrated solar power systems.” *Journal of Solar Energy Engineering* 140 (5): 051011.

Yang, Huiqiang, Ryan C Gallagher, Anh-Thu Phan, Patrice Chartrand, and Aïmen E Gheribi. 2023. “A predictive approach for the compositional and temperature representation of thermal conductivity in multicomponent molten salt systems for advanced energy applications.” *Materials Today Energy* 38:101441.

Yingling, JA, J Schorne-Pinto, M Aziziha, JC Ard, AM Mofrad, MS Christian, CM Dixon, and TM Besmann. 2023. “Thermodynamic measurements and assessments for LiCl-NaCl-KCl-UCl3 systems.” *The Journal of Chemical Thermodynamics* 179:106974.

Yingling, Jacob A, Mina Aziziha, Juliano Schorne-Pinto, Jorge Paz Soldan Palma, Johnathan C Ard, Ronald E Booth, Clara M Dixon, and Theodore M Besmann. 2023. "Thermodynamic Assessment of CrCl2 with NaCl–KCl–MgCl2–UCl3–UCl4 for Molten Chloride Reactor Corrosion Modeling." *ACS Applied Energy Materials* 6 (11): 5868–5882.

Yuan, Haomin, Nathaniel Hoyt, Nadish Saini, Dezhi Dai, Dillon Shaver, Jicheng Guo, and Yu-Hsiang Lan. 2024. *MOSCATO Development and Integration in Fiscal Year 2024.* Technical report. Argonne National Laboratory (ANL), Argonne, IL (United States).